Determination of periodic response limits among multiple solutions for mechanical systems with wedge dampers

Determination of Periodic Response Limits Among Multiple Solutions for Mechanical Systems with Wedge Dampers

Erhan Ferhatoglu , Stefano Zucca

PII: S0022-460X(20)30739-2
DOI: https://doi.org/10.1016/j.jsv.2020.115900
Reference: YJSVI 115900

To appear in: *Journal of Sound and Vibration*

Received date: 3 June 2020
Revised date: 24 October 2020
Accepted date: 4 December 2020

Please cite this article as: Erhan Ferhatoglu , Stefano Zucca , Determination of Periodic Response Limits Among Multiple Solutions for Mechanical Systems with Wedge Dampers, *Journal of Sound and Vibration* (2020), doi: https://doi.org/10.1016/j.jsv.2020.115900

Determination of Periodic Response Limits Among Multiple Solutions for Mechanical Systems with Wedge Dampers

Erhan Ferhatoglu†[1], Stefano Zucca†

† Department of Mechanical and Aerospace Engineering, Politecnico di Torino, Corso Duca degli Abruzzi 24, 10129 Torino, Italy

ABSTRACT

Wedge dampers are commonly used to utilize the frictional behavior in many engineering fields such as vehicle dynamics and turbo-machinery. However, the presence of non-unique contact forces in the damper interfaces creates an uncertainty that provides different dynamic response amplitudes even for the same input parameters. The maximum limits of the variability range always take the core attention in most of the damper design processes. In this paper, determination of an upper and a lower boundary among multiple steady-state solutions is presented by using a numerical approach. The method is specifically suitable for the mechanical systems with wedge dampers modeled by macro-slip frictional contact elements in the joint interfaces. In the approach proposed, a criterion that determines the periodic response boundaries according to the limit tangential force values is utilized. The method is demonstrated by illustrating several case studies on a lumped parameter system which represents a turbo-machinery application with a symmetric wedge damper pressed against two vibrating adjacent blades. A point-to-point 1D friction model with varying normal force is used in both contact sides. A parametric investigation on the variability range and response limits is performed for different damper configurations. Harmonic Balance Method with Newton's iteration scheme is used in the numerical solution of the governing equations. The results show that a large variability exists for damper geometries where a strong coupling is present between tangential and normal contact forces. The method proposed successfully captures the limits of the variability range in all cases.

Keywords: Multiple Solutions, Dry Friction, Variability Range, Periodic Response Limits, Wedge Dampers.

[1] Corresponding Author
E-mail addresses: erhan.ferhatoglu@polito.it (Erhan Ferhatoglu), stefano.zucca@polito.it (Stefano Zucca)

1. INTRODUCTION

Wedge damper is a secondary structure that is implemented for many practical purposes in several engineering fields. One of the mostly used application areas is the turbo-machinery where high cycle fatigue problems due to undesired vibrations take the highest attention in the design phase [1]. A complete detuning of the natural frequencies with respect to the excitation is sometimes impossible for complex structures because of high modal density of the rotors. Thus, mitigation of high vibration amplitudes during operation by exploiting the wedge dampers, which are also known in turbo-machinery as a specific type of the under-platform dampers (UPD), becomes highly favorable [2-4]. Wedge dampers have also been widely used in vehicle system dynamics where some examples are in the modeling of the suspension systems in wagon structures [5, 6], in the assessment of stability problems for complex train systems [7, 8] or in the simulation of the other friction devices such as friction draft gears [9].

Highly sophisticated Finite Element (FE) model of the bodies (bladed disks, gears, UPDs and etc.) allows taking into account the bulk elasticity, while a layer of contact elements should be placed between the joint interfaces to couple the touching pairs in order to simulate the local compliance of the contact region and the additional damping dissipated. The first models have been proposed more than five decades ago as a one dimensional bilinear hysteretic restoring force technique [10], which has pioneered to develop new studies. Coulomb friction model is then proposed for a 1D motion between the blade and the damper [11, 12]. For a more accurate response, 2D [3, 13, 14] and 3D [15] motions are taken into account in different models. Readers may refer to [16] and [17] for a more detailed investigation about the wedge damper applications and contact models used in the vehicle dynamics and in the turbo-machinery, respectively.

Apart from the contact models, a common sense in the numerical solution procedures was to separate the static and dynamic parts of the governing equations, which is the so-called uncoupled approach. In this technique, a quasi-static analysis by excluding the dynamic excitations is firstly performed in order to calculate the static normal loads due to assembly pre-loads or the centrifugal force during rotation on the joint interfaces. Then, the dynamic part of the vibratory response problem is separately solved in a second step by taking previously computed static normal loads as input. The uncoupled approach is generally used for a better robustness and convergence in the numerical solution scheme. However, it is proven numerically that simultaneous solution of the static and the dynamic parts in the harmonic balance equations gives much more accurate results [18, 19]. Pesaresi et al. [20]

also showed that experimental results of contact interfaces under large normal load variation only match with the analysis solutions if the coupled approach is used in the numerical solution scheme. Most of the real life applications with wedge dampers operate under a remarkable variation of normal loads with a large force distribution over the contact area during vibration cycle. In these cases, the mean component of the oscillatory damper response considerably shifts especially around the resonance frequencies. This natural behavior of the damper necessitates the inclusion of the zeroth order harmonic together with the higher orders in the solution algorithm, i.e. coupled approach, in order to be able to predict the dynamic response truly.

Coupled approach provided an insight to researchers and engineers to explore an uncertainty phenomenon which is firstly introduced to structural dynamics community by Yang et al. more than two decades ago [21, 22]. The authors have studied the uncertainty phenomenon of the contact forces in the wedge dampers, where multiple responses are possible even if all the system parameters and inputs are kept same. It is shown that different contact states and initial values of the friction forces in the beginning of the simulation may lead to non-unique response amplitudes when steady-state is reached. However, the authors have also reported in the same study that experimental values did not vary for different tests, which shows a discrepancy between the real observation and the theory. This contradiction is then explained with the fact that the damper in the experiments is reloaded for each run, which caused to obtain free interfaces, i.e. zero initial friction force, at the beginning of the tests. Consequently, the same initial conditions have been unintentionally imposed and no multiple responses are obtained. Uncertainty phenomenon is later numerically shown in UPDs by Zucca et al. [23], where a variability range is possible in the response calculations. This phenomenon has been investigated in different studies of the bladed disk applications with UPDs [18, 24] and mid-span dampers [25]. A very recent study [26] also numerically showed that co-existing system solutions for friction-induced vibrations result multiple steady-state responses for different initial conditions. In order to investigate the damper dynamics in laboratory conditions, Botto et al. [27] designed a novel test rig for the characterization of the UPDs. Keeping all the system properties and inputs fixed, the experiment has been performed consecutively with different initial loading sequences of the same static load, which affects the first state of the damper before starting to each test. Firstly, a monotonically loading sequence of dead weights is applied until to reach a pre-determined static target value that represents the centrifugal static force; on the other hand, in the second run, the target value is

first exceeded and the dead weights are then removed. It is shown that multiple responses are physically possible in this way by performing successive tests with the identical input parameters for the same structure. Similarly, Gastaldi et al. [28] observed a very large scattering of dynamic response in the experiments of UPDs. The authors have stated that the large variability of oscillation amplitudes in successive tests cannot be explained with micro changes observed in contact surfaces (micro-wear) since they gradually evolve in time. All of these experimental observations prove that uncertainty phenomenon is not a modeling artifact and does not depend on the contact models used in the numerical analyses.

Determination of an upper and a lower boundary of multiple responses may play an important role from the engineering point of view in the dynamic design process since the mechanical parts are generally designed with respect to their maximum dynamic amplitudes obtained at resonance frequencies for different excitation levels. For this purpose, Yang et al. [21, 22] had investigated the uncertainty phenomenon for the wedge dampers with two interfaces, where each side is modeled with a single point contact element. The authors offer an analytical approach for the computation of two extreme friction force trajectories if they exist, in which the geometric relations in stick–slip configurations are utilized. The derivation of this approach in detail can be found in [29]. Zucca et al. [24] also offered a technique to obtain always the same single response curve among an infinite number of options. However, to the best of the authors' knowledge, a generalized approach for the determination of the boundaries for the applications including several contacts is not available in the literature.

In this paper, a numerical approach that enables to obtain the upper and the lower periodic response limits among multiple solutions for mechanical structures including frictional contacts with wedge dampers is offered. Contact behavior on both damper sides is modeled by using the state-of-art 1D macro-slip friction element model with varying normal force. Modeling the contact behavior by using a single point in each damper side has been widely performed in the past [21, 22, 30, 31], where several contact elements are then included in the models to be able to increase precision with developing advances. This study offers the first numerical technique for the determination of the upper and the lower limits and constructs a structural framework for further studies. The method specifically utilizes the use of limit tangential forces imposed by Coulomb's friction law in the fully stuck damper side, which provides to obtain the maximum and the minimum normal load on the other side that makes an alternating stick–slip or an alternating stick–slip–lift-off motion. In this way, two extreme contact cases in slipping side, which simulate the closest ones to open and fully stuck

conditions, are obtained. Hence, the response limits within the variability range are computed. The method is demonstrated by using a lumped parameter system simulating a simplified model of the two adjacent blades with a wedge damper imposed in between them. Several case studies and a parametric investigation for different damper geometries have been presented by using the proposed approach. It is shown that even though the variability range is considerably affected by the geometry of the damper, the method is able to obtain the limits for all cases. In the solution process, Harmonic Balance Method is utilized by transforming the governing differential equations into frequency domain and the numerical solution is then obtained by using Newton-Raphson approach with successive iterations. Despite the model simplicity, the authors believe that this study creates a fundamental infrastructure and may help the analysts in the design of the mechanical parts with highly detailed FE models. It is also worth mentioning that although the approach offered in this paper is for the wedge damper applications, it can also be extended to the other applications that exploit dry friction damping, since the uncertainty phenomenon is a general fact and cannot be confined for a specific case.

2. BACKGROUND

2.1 Governing Equations

Consider the differential equation of a vibrating structure with joint interfaces under a periodic excitation force as

$$\mathbf{M}\ddot{\mathbf{q}}(t)+\mathbf{C}\dot{\mathbf{q}}(t)+\mathbf{K}\mathbf{q}(t)+\mathbf{F}_c(t)=\mathbf{F}_{exc}(t)\,. \tag{1}$$

$\mathbf{M}$, $\mathbf{C}$ and $\mathbf{K}$ represent the linear system matrices of mass, viscous damping and stiffness, respectively. $\mathbf{q}(t)$ is the vector of generalized coordinates in time domain. $\mathbf{F}_c(t)$ and $\mathbf{F}_{exc}(t)$ are the vectors of internal nonlinear contact forces and external periodic excitation forces, respectively.

In case of seeking the steady-state solution of the structure; the general response, contact forces and excitation forces can be assumed as an expression of a truncated series as

$$\mathbf{q}(t)=\mathrm{Re}\left(\sum_{h=0}^{H}\hat{\mathbf{q}}^h e^{ih\omega t}\right),\quad \mathbf{F}_c(t)=\mathrm{Re}\left(\sum_{h=0}^{H}\hat{\mathbf{F}}_c^h e^{ih\omega t}\right)\quad\text{and}\quad \mathbf{F}_{exc}(t)=\mathrm{Re}\left(\sum_{h=0}^{H}\hat{\mathbf{F}}_{exc}^h e^{ih\omega t}\right), \tag{2}$$

respectively. Here, $\hat{\mathbf{q}}^h$, $\hat{\mathbf{F}}_c^h$ and $\hat{\mathbf{F}}_{exc}^h$ stand for the complex amplitude vectors corresponding to the h^{th} harmonic. In addition, H, ω and i represent the number of harmonics considered in the expansion, excitation frequency and unit imaginary number, respectively. After inserting all the expressions defined in Eq. (2) into Eq. (1) and cancelling the similar terms on both sides, a set of nonlinear algebraic equations in frequency domain is obtained as

$$\left(-(h\omega)^2\mathbf{M}+ih\omega\mathbf{C}+\mathbf{K}\right)\hat{\mathbf{q}}^h+\hat{\mathbf{F}}_c^h-\hat{\mathbf{F}}_{exc}^h=\mathbf{0} \qquad (h=0,1,\cdots,H), \tag{3}$$

where both the static (h = 0) and the dynamic (h = 1$\cdots H$) balances are coupled to each other through the nonlinear contact forces, $\hat{\mathbf{F}}_c^h$, which directly depend on the response of the system, $\hat{\mathbf{q}}^h$.

2.2 Contact Model and Computation of Internal Forces

In this paper, a point contact element, the so-called Jenkins element as shown in Fig. 1, is utilized to model the contact behavior. In this approach, the contact element has a tangential and a normal direction perpendicular to each other, in which the contact forces are generated as Tangential Force, *T*, and Normal Force, *N*, respectively. A slider in tangential direction is used to attach two contact points at joint interfaces. In case of a variable normal load application, which is the general situation in most of the real life applications, the local contact stiffness of the touching points is simulated using two linear springs, with the stiffness values of k_t and k_n, employing in tangential and normal directions, respectively.

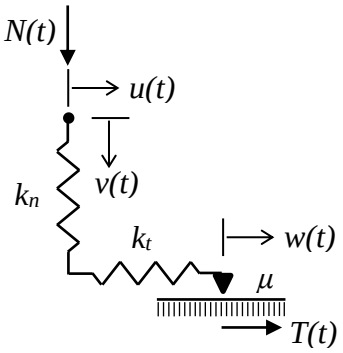

Fig. 1 Point Contact Element

Coulomb friction law states that Tangential Force, *T(t)*, must be equal or lower than the limit value of $\mu N(t)$, being μ the friction coefficient, when the slider sticks. It starts slipping with respect to the ground with an amount of slip motion, *w(t)*, when tangential force exceeds the limit value. The periodic relative tangential displacement, *u(t)*, and the periodic relative normal displacement, *v(t)*, of contact points determine the tangential and the normal forces for

each contact element. The normal and the tangential contact forces at any time t is defined as follows

$$N(t) = \max\left(k_n v(t), 0\right) \quad , \quad T\left(t\right) = \begin{cases} k_t\left[u(t) - w(t)\right] & \text{stick state} \\ \mu N(t)\text{sign}\left(\dot{w}(t)\right) & \text{slip state} \\ 0 & \text{lift-off state} \end{cases} . \tag{4}$$

It can be seen from Eq. (4) that $N(t)$ cannot take negative values. Because, contact element gets separated due to the unilateral boundary condition at the contact point in case of having negative relative normal displacements. The tangential contact force also takes different values with respect to the corresponding contact state. It should be noted in Eq. (4) that the position of the slider, $w(t)$, for a specific time instant t is an unknown parameter in advance. This fact does not enable the actual value of the tangential force to be directly computed. In order to overcome this problem, a four step predictor-corrector approach [32] can be followed in the calculation procedure as follows;

1- The contact is assumed in the stick condition at time t.

2- The value of the tangential force can be estimated by using an arbitrary slip motion value, $w(t)$. One of the best options among many values can be the one computed at the previous time step, $w(t - \Delta t)$, as follows

$$T^P(t) = k_t\left[u(t) - w^P(t)\right] = k_t\left[u(t) - w(t - \Delta t)\right]. \tag{5}$$

Here, $T^P(t)$ and $w^P(t)$ represent the predicted values of the tangential contact force and slip motion at time t, respectively. Δt is the time step.

3- The assumption made in step 1 is checked by comparing the value of the predicted tangential force with the limit value $\mu N(t)$ whether it is correct or not. If the predicted tangential force value does not exceed the limit value, i.e. neither slip nor separation occurs, the assumption is valid and the contact is in stick state. Otherwise, it is not.

4- If the assumption holds with respect to criteria defined in Step 3, the tangential force value predicted in Step 2 becomes correct. However, if it is wrong, which means the true condition is slip or separation, the correct value with respect to the corresponding contact state is assigned as shown in Eq. (4). As a summary, the corrector step for the tangential force, $T(t)$, and the slider displacement, $w(t)$, can be written with a more general expression as

$$T(t)=\begin{cases} T^P(t) & \text{stick} \\ \mu N(t)\text{sign}\left(T^P(t)\right) & \text{slip} \\ 0 & \text{lift-off} \end{cases}, \quad w(t)=\begin{cases} w(t-\Delta t) & \text{stick} \\ u(t)-\mu N(t)\text{sign}\left(T(t)\right)/k_t & \text{slip} \\ u(t) & \text{lift-off} \end{cases}. \quad (6)$$

It should be noted that when compared to analytical calculation of contact forces [33], predictor-corrector approach apparently brings much more simplicity accompanying with some inaccuracy in the determination of transition points between contact states. Nonetheless, the error can be minimized by keeping the time step size low enough [34] and can be reduced to a negligible level from the point of engineering view.

Contact force values calculated by using Eq. (4) are still in time domain. However, as shown in Eq. (3), the final set of nonlinear algebraic equations requires the computation of Fourier coefficients. In this study, internal nonlinear contact forces, $\hat{\mathbf{F}}_c^h$, are computed by using the Alternating Frequency/Time approach [35]. In this technique, time histories of the relative displacements, $u(t)$ and $v(t)$, are calculated by taking the Inverse Fast Fourier Transform (IFFT) of Fourier coefficients, $\hat{u}^h$ and $\hat{v}^h$. Periodic internal contact forces are then computed with the contact model by using Eq. (4). Finally, Fast Fourier Transform (FFT) is applied to contact forces computed in time domain, $T(t)$ and $N(t)$, to obtain their corresponding Fourier coefficients in frequency domain, $\hat{T}^h$ and $\hat{N}^h$, respectively. AFT approach is also summarized in Fig. 2.

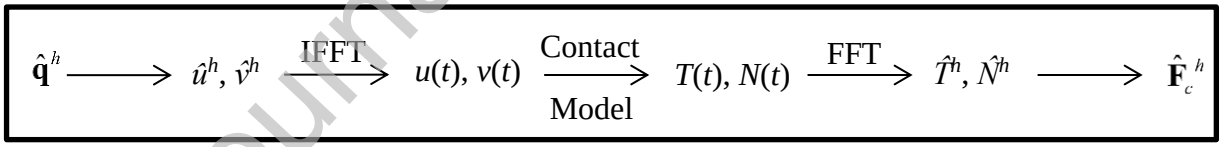

Fig. 2 Alternating Frequency/Time Approach

2.3 Solution Process

The set of nonlinear algebraic Eq. (3) can be numerically solved by using Newton-Raphson Method with Pseudo-Arc-length Continuation [36]. It should be noted that since the equation set is coupled through contact forces, the solution procedure requires a successive iteration scheme. In the solution approach utilized, frequency, ω, is also another additional parameter to be determined other than the complex coefficients of unknown response vector, $\hat{\mathbf{q}}^h$. The residual of Eq. (3) is defined as

$$\mathbf{R}\left(\hat{\mathbf{q}}^h,\omega\right)=\left(-(h\omega)^2\mathbf{M}+ih\omega\mathbf{C}+\mathbf{K}\right)\hat{\mathbf{q}}^h+\hat{\mathbf{F}}_c^h-\hat{\mathbf{F}}_{exc}^h \quad (h=0,1,\cdots,H). \quad (7)$$

The convergence can be assured by decreasing the residual values under a pre-specified tolerance value. Iteration scheme for the current solution point can be written as

$$\mathbf{p}_{j+1} = \mathbf{p}_j - \begin{bmatrix} \dfrac{\partial \mathbf{R}(\mathbf{p}_j)}{\partial \hat{\mathbf{q}}_j^h} & \dfrac{\partial \mathbf{R}(\mathbf{p}_j)}{\partial \omega_j} \\ \dfrac{\partial \mathbf{h}(\mathbf{p}_j)}{\partial \hat{\mathbf{q}}_j^h} & \dfrac{\partial \mathbf{h}(\mathbf{p}_j)}{\partial \omega_j} \end{bmatrix}^{-1} \times \begin{Bmatrix} \mathbf{R}(\mathbf{p}_j) \\ \mathbf{h}(\mathbf{p}_j) \end{Bmatrix} \tag{8}$$

where

$$\mathbf{p}_j = \begin{Bmatrix} \hat{\mathbf{q}}_j^h \\ \omega_j \end{Bmatrix} \quad \text{and} \quad \mathbf{h}(\mathbf{p}_j) = \mathbf{z}^T \left(\mathbf{p}_j - \mathbf{p}_p \right). \tag{9}$$

$\mathbf{h}(\mathbf{p}_j)$ denotes the new equation to be added to the system of equations. Additionally, j, $\mathbf{z}$ and $\mathbf{p}_p$ represent the iteration number, the unit vector that is tangent to the solution curve and predicted unknown vector before starting iterations, respectively. Numerical solution of the nonlinear equations with the Newton-Raphson Method requires calculating the Jacobian Matrix in each iteration. In this study, this matrix is computed numerically by utilizing forward finite difference method. Readers may refer to [37] for more detailed information about the Newton-Raphson Method with Pseudo-Arc-length Continuation.

2.4 Dynamic Behavior of Structures with Friction Contacts

In this section, a general dynamic behavior of mechanical structures with friction contacts under a periodic excitation is briefly recapped. Due to the nonlinear nature of the contact, the response of the structure strongly depends on the excitation amplitude and the static forces, also called as pre-loads, which keep the bodies in contact during the system vibration. The typical steady-state vibration amplitude plot around one of the system resonances without having a modal interaction or internal resonances is given in Fig. 3a. Each curve corresponds to a different value of the static pre-load. It is observed that as the static pre-load, N_0, increases:

1- The maximum response point decreases up to a minimum value corresponding to the system response with an optimal pre-load and then increases again.

2- The resonance frequency increases up to a final value that is equivalent to the dynamics of the system with fully stuck contacts.

The optimal curve, which is obtained by assembling the maximum response points of each response graph with respect to increasing static pre-load, is also depicted in Fig. 3b. In general, as the static normal force (pre-load) decreases, the structures tend to a configuration that corresponds to the linear structure with open contacts; while as the static normal force increases, the structures tend to a configuration that corresponds to the linear structure with fully stuck contacts.

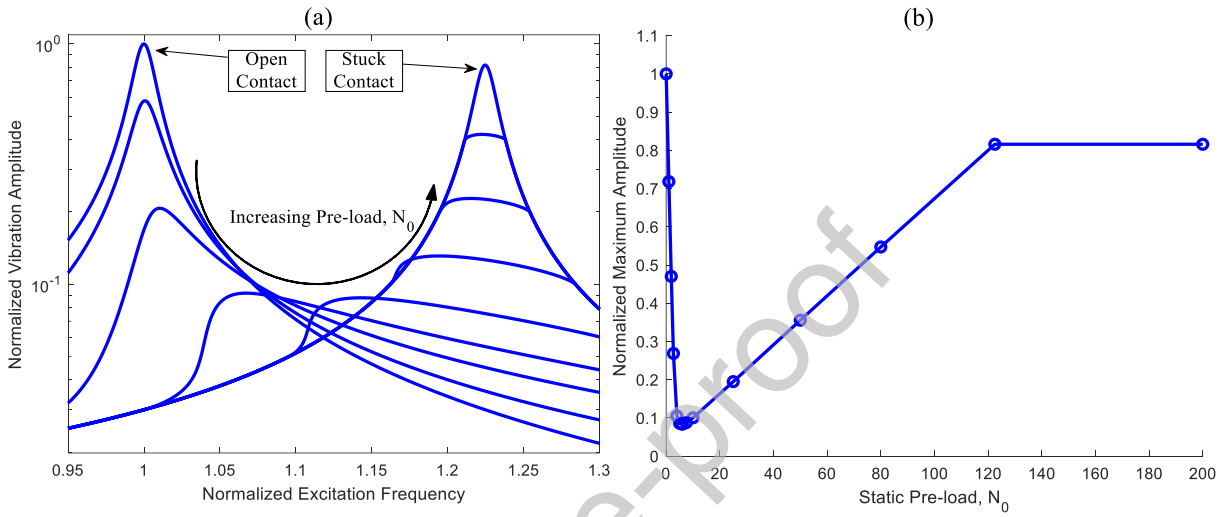

Fig. 3 (a) Typical Effect of Static Pre-Load on the Dynamics of Structures with Friction Contacts, (b) Optimal Curve of a Structure with Friction Contacts

To further explain the behavior observed in Fig. 3a and Fig. 3b, consider a single Jenkins element under a given periodic motion, $\mathrm{q}(t)$. Internal nonlinear force by dry friction, $\mathrm{f}_c(t)$, for the steady state motion can be expressed in a more general way as

$$\mathrm{f}_c(t) = \left(\mathrm{k}_{eq}(\hat{q}) + i\mathrm{c}_{eq}(\hat{q})\right) \times \mathrm{q}(t) \ , \tag{10}$$

where $\hat{q}$ represents the response amplitude. k_{eq} and c_{eq} are the effective stiffness and the equivalent damping terms of the contact element, respectively. General expression of internal nonlinear forces with a multiplication form as shown in Eq. (10) is first used in [38] and then generalized in [39] by defining complex describing functions that physically correspond to the effective stiffness and the equivalent damping terms of the nonlinearities for a certain harmonic input motion. The real and imaginary parts of the describing functions represent k_{eq} and c_{eq}, respectively, and their analytical expression for a 1D dry friction element which is under a single harmonic input motion with a constant normal load, N_0, is given in Appendix. These quantities, which are representatively plotted in Fig. 4, determine the contact elements'

overall dissipative characteristics, which directly depend on the state conditions that the contact elements undergo during the full cycle. As can be seen in Fig. 4a, k_{eq} starts from zero and saturates at a specific value, which means that the contact element becomes effective in the system with increasing pre-load and shifts the response graph from free linear case to the fully stuck linear case by adding stiffness to the structure. The contact state then becomes fully stuck after a certain pre-load and k_{eq} becomes equal to the contact stiffness value. On the other hand, in Fig. 4b, c_{eq} takes its maximum value for an intermediate pre-load that is defined as the so-called optimum point. After this point, the damping ability of the contact element decreases with increasing static pre-load and becomes zero at the fully stuck state condition.

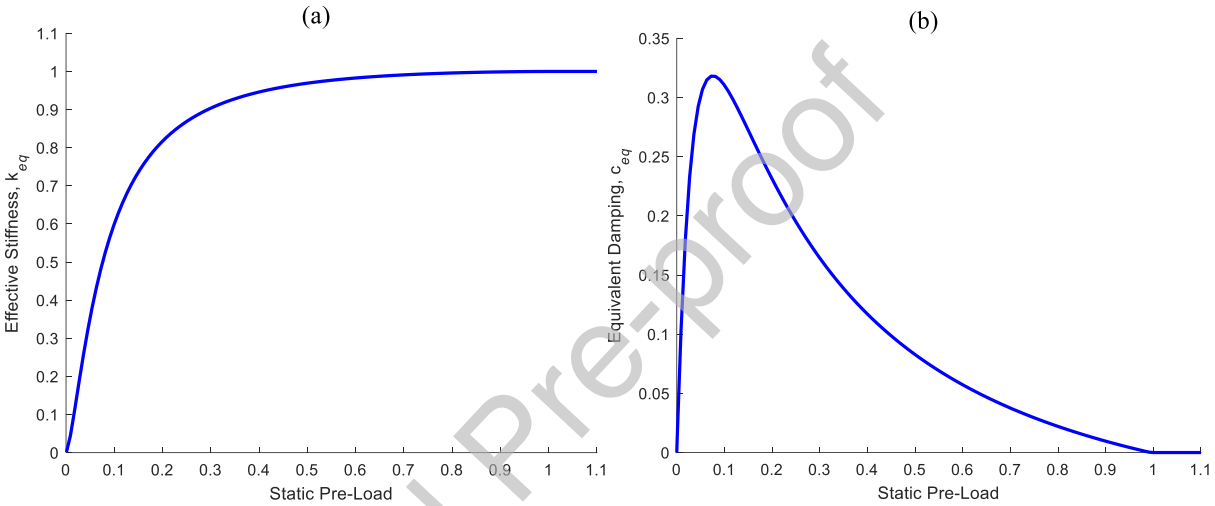

Fig. 4 (a) Effective Stiffness and (b) Equivalent Damping for a Dry Friction Element

3. METHODOLOGY

3.1 Variability of the Tangential Force

Wedge dampers generally work under the conditions where large normal force variation takes place due to variable normal relative displacements between the damper and the blade platforms. For instance, in turbine bladed disks applications, the damper may even experience a loss of contact around the resonance frequencies of the first flexural in-phase mode due to blade dynamics [20]. Therefore, taking into account the varying normal load is essential in the contact modeling. Let's consider a generic Jenkins element with a variable normal load and assume a case where the input motion is relatively small so that the contact element has a stick state for the entire cycle. The resulting tangential force, $T(t)$, in this case must always be bounded by an upper ($\mu N(t)$) and a lower ($-\mu N(t)$) limit imposed by the Coulomb's friction law. However, it should be noted that the static value of the tangential force computed, T^0, can vary within a range ($T^0_{min} \leq T^0 \leq T^0_{max}$). The limits for this range are determined by the static

parts of maximum ($T_{max}(t)$) and minimum ($T_{min}(t)$) tangential forces, which make tangent to the positive and negative Coulomb's limit values, respectively. The variability range is representatively shown with corresponding time histories and hysteresis curves in Fig. 5. It can be easily inferred that there is an infinite number of contact force curves that can be obtained within this range. It is worthy to note that although the static value differs for each curve, all of them must have the same dynamic components since the variable part of tangential force is directly determined by the harmonic components of the input motion. This fact creates a non-uniqueness phenomenon in the calculation of the tangential force for a fully stuck state. It should also be noted that although a varying normal is considered for this representative particular case, non-uniqueness of the static tangential force, within the range between T^0_{min} and T^0_{max}, also exists for contacts that exhibit a constant normal load.

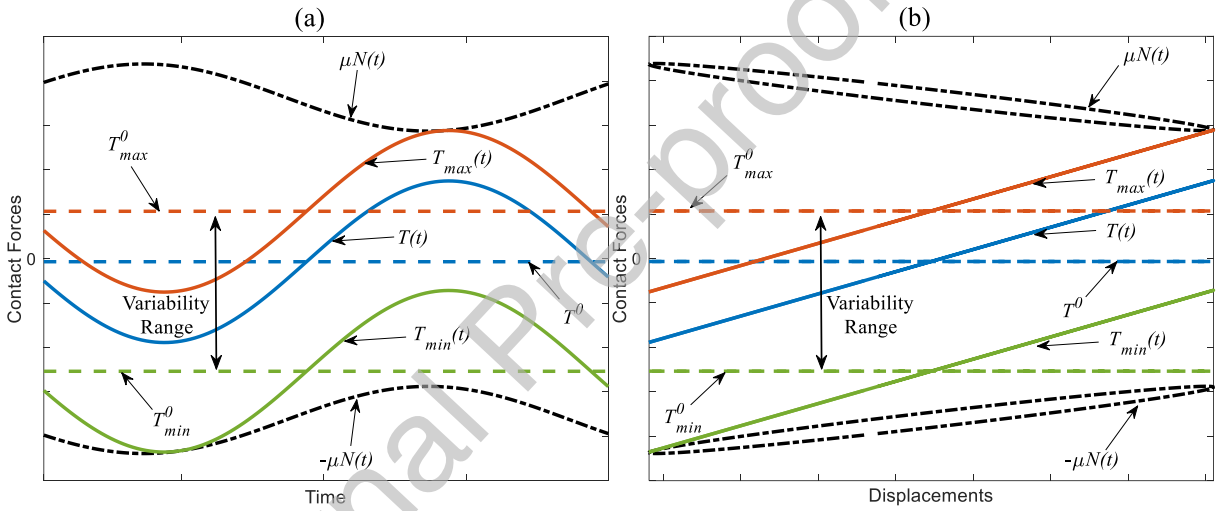

Fig. 5 (a) Time Histories and (b) Hysteresis Curves for a Full Stick Cycle

In order to clarify the situation further, consider Fig. 6a showing the Jenkins contact element that is under a fully stuck condition with the given input motion, *u(t)*. The tangential force for a stick state can be computed by using the formula given in Eq. (4) which also includes the slider motion, *w(t)*. However, since the coordinate of the slider is an unknown parameter in advance, it can be hypothetically positioned within a range in such a way that the contact is always going to be in the stick state, as shown in Fig. 6b and Fig. 6c, in which the upper and lower limits are the points where positive and negative slips are about to initiate. Since any position between two limits is acceptable, an infinite number of periodic function *T(t)* then exist, as indicated in Fig. 5.

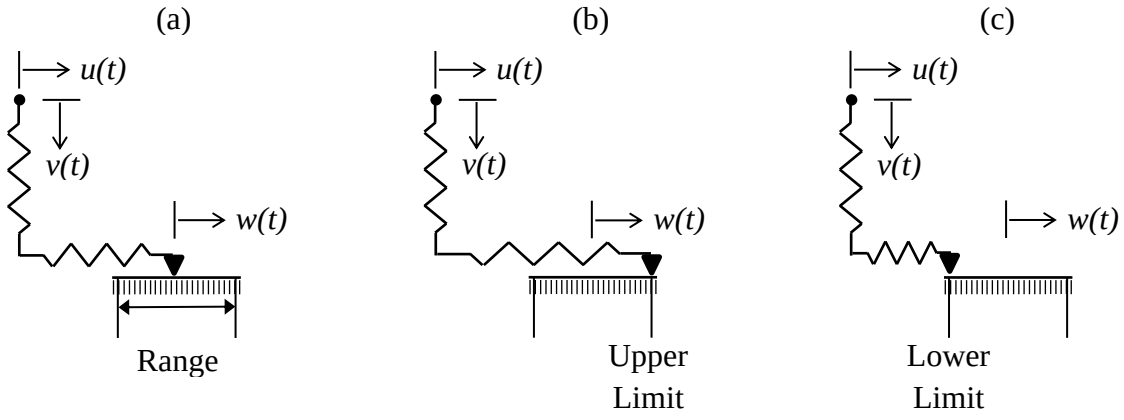

Fig. 6 Contact Element with Different Slider Positions

It is also worth noting that non-unique values of the tangential contact force only occur for the fully stuck cycle. In case of an alternating stick–slip or an alternating stick–slip–lift-off cycle, only one single value for T^0 can be computed due to the fact that tangential force has already been confined by the limit. For example, consider Fig. 7, which shows the time histories and hysteresis curve for an alternating stick–slip cycle. Tangential force starts to cycle in the negative slip state and directly takes the lower limit value. After transition to stick state, which is the time instant shown with blue dot, there is only one unique curve for the tangential force, which removes the uncertainty. Then, the condition again changes from stick to positive slip and this alternating motion continues until the end of the cycle. Similar behavior can be observed also for an alternating stick–slip–lift-off cycle as depicted in Fig. 8, where the transition points between slip and lift-off states are shown with black dots. As a result, contact forces of a single Jenkins element are uniquely computed for both these cases. Hence, the uncertainty of the non-unique tangential contact force only exists for the contacts remaining fully stuck during the vibration cycle, i.e. the uncertainty in the system only exists if at least one of the contact points remains stuck during the vibration cycle.

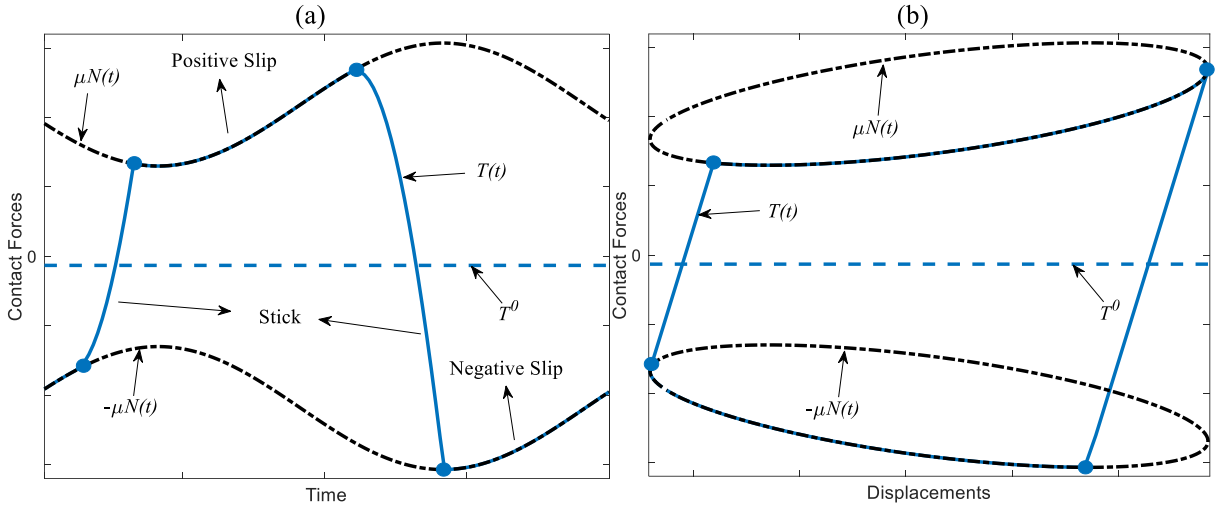

Fig. 7 (a) Time Histories and (b) Hysteresis Curve for an Alternating Stick–Slip Cycle

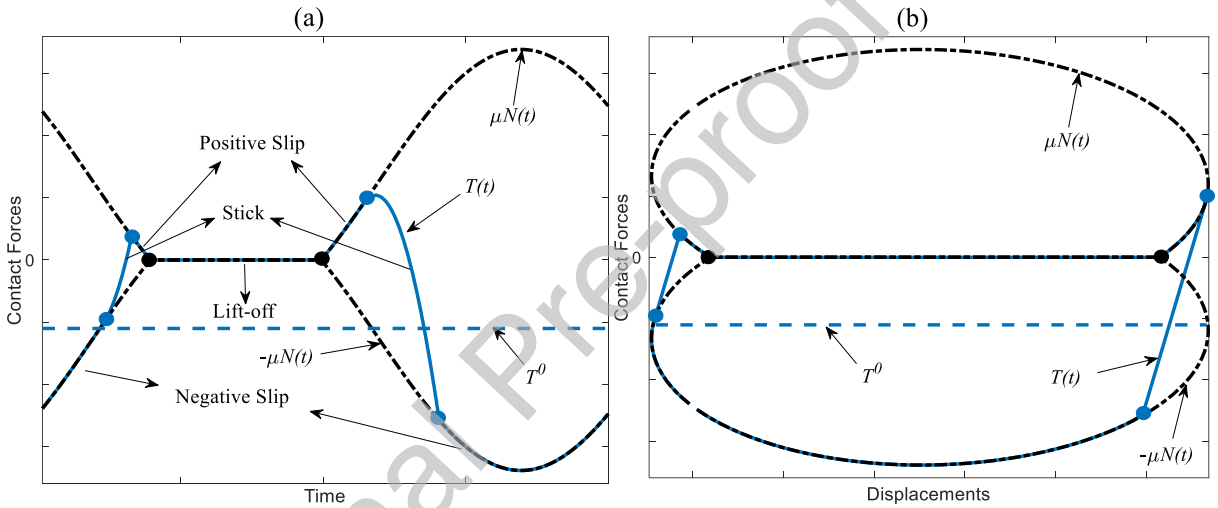

Fig. 8 (a) Time Histories and (b) Hysteresis Curve for an Alternating Stick–Slip–Lift-off Cycle

3.2 Multiple Responses of Mechanical Systems with Wedge Dampers

The uncertainty phenomenon of the tangential force may enable the mechanical structures including contacts to exhibit a variable frictional characteristic. This fact can be much more impactful in the applications of wedge dampers as investigated in [21-24, 27, 28, 40]. In this paper, the attention is focused on the frictional systems with wedge dampers despite the fact that uncertainty phenomenon is a general matter of fact for engineering systems with dry friction.

Consider a mechanical system with an asymmetric wedge damper pressed between two vibrating bodies as shown in Fig. 9a. Each damper side can be coupled to the adjacent body by means of a Jenkins element.

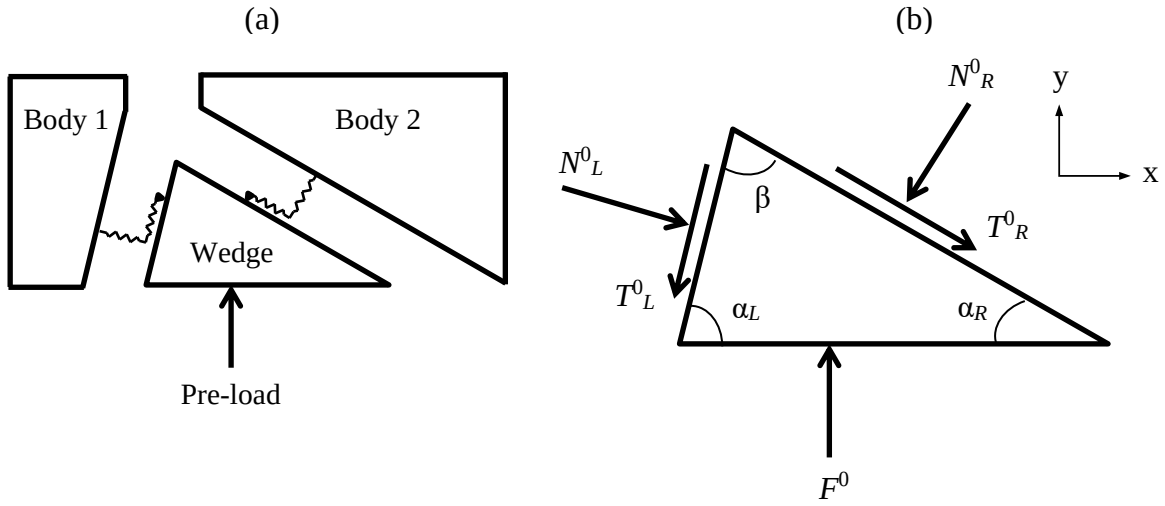

Fig. 9 (a) An Asymmetric Wedge Damper Pressed Between Two Inclined Surfaces, (b) Static Forces Acting on the Damper

Assuming the system is under a periodic excitation, three different contact conditions can be achieved during the steady-state motion. These cases can be as follows;

1- Both sides may be fully stuck.

2- Both sides may undergo an alternating stick–slip cycle or an alternating stick–slip–lift-off cycle.

3- One side may be under fully stuck case, while the other one shows an alternating stick–slip or an alternating stick–slip–lift-off behavior.

In case 1, there is an uncertainty in the static tangential force on both sides. However, the system behaves as a linear system. Hence, this case provides no friction damping to the system, which leads to obtain a unique vibration amplitude.

In case 2, static tangential forces are uniquely defined on both sides as shown in Fig. 7 and Fig. 8. Hence, there is no variability in the contact forces, which enables to obtain only one unique response, as well.

In case 3, the static tangential force on the fully stuck side is not uniquely defined while the one for the other side is unique. In order to investigate this case further, consider the static force balances on the wedge damper in x and y directions, which are representatively shown in Fig. 9b. They can be written for this configuration as

$$\begin{aligned} {T^0}_R\cos(\alpha_R) - {N^0}_R\sin(\alpha_R) - {T^0}_L\cos(\alpha_L) + {N^0}_L\sin(\alpha_L) = 0 \\ {T^0}_R\sin(\alpha_R) + {N^0}_R\cos(\alpha_R) + {T^0}_L\sin(\alpha_L) + {N^0}_L\cos(\alpha_L) = F^0 \end{aligned} . \quad (11)$$

For the simplicity, assume, without any loss of generality, that the left damper side (with subscription *L*) is in full stick cycle while the right damper side (with subscription *R*) shows an alternating stick–slip or an alternating stick–slip–lift-off behavior. It can be clearly inferred that the uncertainty in ${T^0}_L$ directly affects the system behavior with the coupling that is present in Eq. (11). Different values of ${T^0}_L$ result non-unique ${N^0}_R$, which leads to obtain a variable steady-state k_{eq} and c_{eq} for the right side of the damper due to different normal load values. This makes the dynamic behavior of the system to have a variable pattern as if the structure is forced by the same dynamic excitation but with different static loads. Because, simultaneous solution of Eq. (7) provides a coupling between the static and the dynamic parts. As a result, multiple solutions of the system eventually exist for case 3.

Although an illustration for the presence of multiple responses is explained here for a very simple case of wedge dampers modeled without considering the rotational effects and using two Jenkins elements, the uncertainty might occur even in case of a more complicated damper kinematics with multiple contact elements. It should be noted that the amount of uncertainty is system dependent. For example, there may be even 50 Hz resonance frequency difference between multiple responses obtained after two consecutive experiments as reported in [28]. Moreover, ten times difference among multiple amplitudes at the same frequency is possible in industrial turbine bladed disks with mid-span dampers [25]. Therefore, the uncertainty phenomenon is not a modeling artifact and it comes from the nature of frictional behavior as experimentally shown in [27, 28, 40].

3.3 Response Limits

Numerical computation of multiple responses and the determination of upper and lower limits would take an interest in the design phase of the wedge dampers. Particularly, the upper bound at the resonance frequency may play the most important role from the engineering point of view. In this paper, in order to predict the range of the response level associated to the case 3 mentioned in the previous section, an approach, which is able to provide the limit response curves that bound the multiple responses, is developed based on the following observations:

1- As a general fact, the physics of a slipping contact behavior implies that the contact approaches to the fully stuck condition if the static normal load exerted in normal direction increases. On the other hand, the lower the static normal load is, the closer the contact will be to the free condition, i.e. no friction forces. (see Fig. 3)

2- As mentioned in Section 2.4, the free and the fully stuck contact configurations determine the two limit dynamic configurations of the nonlinear system.

3- As mentioned in Section 3.2, the static normal load acting on the right slipping side of the damper, N^0_R, has non-unique values because of the cross-coupling between the two damper sides.

For the above mentioned reasons, it can be clearly concluded that the two configurations corresponding to the minimum and the maximum values of the static normal load over the slipping side (N^0_R in this case) determine the boundaries of the response variability range at each excitation frequency. From the static force balances given in Eq.(11), N^0_R can be derived as either

$$N^0_R = \frac{F^0 \sin(\alpha_L) + T^0_R \cos(\alpha_L + \alpha_R) - T^0_L}{\sin(\alpha_L + \alpha_R)} \tag{12}$$

or

$$N^0_R = F^0 \cos(\alpha_R) - N^0_L \cos(\alpha_L + \alpha_R) - T^0_L \sin(\alpha_L + \alpha_R). \tag{13}$$

It is known that the static tangential force on the left damper side, T^0_L, is not unique due to the uncertainty phenomenon. It should be noted that Eq. (12) or Eq. (13) cannot be solved alone since there are three unknowns in each one. However, the relationship between N^0_R and T^0_L is directly related through a divider or a multiplier factor of $\sin(\alpha_L+\alpha_R)$. It is also known for a wedge damper that $0 < \alpha_L+\alpha_R < \pi$, which shows the factor, $\sin(\alpha_L+\alpha_R)$, always takes positive values. As a result, the maximum value of the slipping side's normal load, $N^0_{max,R}$, corresponds to the minimum value of the sticking side's tangential force, $T^0_{min,L}$. Similarly, the minimum value of the slipping side's normal load $N^0_{min,R}$ corresponds to the maximum value of the sticking side's tangential force, $T^0_{max,L}$. Consequently, the boundaries of the response variability range, which are directly determined by the minimum and the maximum values of the static normal load over the slipping side, can be obtained by imposing the limit

values of the static tangential force, T^0_{max} and T^0_{min}, in the calculation of $T(t)$ on the sticking side.

It should be noted that the tangential force limits are unknown in advance before starting the computation of contact forces. However, it is known that $T(t) \equiv m \times \mu N(t)$, where m is bounded in [-1,1] due to Coulomb's law for any t if there is no separation. In order to ensure to have the maximum tangential force limit, $T_{max}(t)$, at steady-state, as also followed in this study, a large enough initial guess value for the tangential force, $T_{ini}(t)$, in the computation of the contact force procedure can be assigned at the very beginning. Numerically, since the limits are always bounded by the normal force components, $\mu N(t)$, in fully stuck conditions, initial prediction of the tangential force, $T_{ini}(t)$,can be set equal to at $t = t_{ini}$ as

$$T_{ini}(t_{ini}) = \mu N(t_{ini}). \tag{14}$$

Then, state-by-state simulation with the predictor-corrector approach, which is explained in Section 2.2 to calculate internal friction forces, will ensure that $T(t)$ is going to end up as $T_{max}(t)$ at steady-state. From the physical point of view, this is the case where the steady state slider position of contact element, $w(t)$, is forced to stay at the farthest point just before the positive slip with respect to the relative displacement coordinate, $u(t)$, as shown in Fig. 6b. On the contrary, the minimum force limit, $T_{min}(t)$, can be obtained with a similar procedure by initially assigning a sufficiently small value, numerically as

$$T_{ini}(t_{ini}) = -\mu N(t_{ini}). \tag{15}$$

This corresponds to a case that the steady state slider position is forced to stay at the farthest point just before the negative slip with respect to the relative displacement coordinate as shown in Fig. 6c.

Another straightforward way to obtain the limits is to assign the static part of the tangential force, T^0, as the maximum, T^0_{max}, or minimum, T^0_{min}, value at the end of the predictor-corrector algorithm within the range as shown in Fig. 5. It should be noted that the contact element should be under fully stuck condition after reaching to steady state to be able to use this approach.

Dynamic response boundaries among multiple solutions can be determined by using the numerical method offered with this study for mechanical systems with wedge dampers modeled by utilizing two point contact elements. Although the analysis of structures with

more than two contact elements are out of scope in this study, multiple contact points might be modeled on each damper side in more realistic applications. For these cases, the number of contact points in fully stuck conditions may become higher than one and the range of the uncertainty gets affected by several elements. The response boundaries may then be determined by some interior tangential forces of fully stuck elements, not by the limits, T^0_{max}, or T^0_{min}. These cases create theoretically an infinite number of possibilities to be able to detect the boundaries, which is impossible to find them manually in reality, and the search for the response boundaries can be a more challenging numerical process. The authors of this study think that the uncertainty phenomenon and the variability of dynamic response studies are open research areas and require further investigations. Nonetheless, this study offers the first numerical approach to detect the response boundaries. In the following section, the application of the proposed approach is presented by means of a simple hypothetical system that imitates a turbo-machinery application with wedge dampers. Multiple response amplitudes with the upper and lower limits are shown if they exist. The effect of different configurations on multiple responses has also been investigated.

4. APPLICATION

In this section, a simplified model representing one of the most common types of friction dampers in turbo-machinery applications, wedge dampers, is studied.

4.1 Lumped Parameter System

The model investigated is constructed using an assembly with three lumped masses simulating two adjacent blades and a wedge damper interposed in between them as shown in Fig. 10. The model utilized is a 6 degree-of-freedom (DOF) system where each mass has two different generalized coordinates allowing the horizontal and the vertical displacements in global x and global y directions, respectively. Two bodies with a mass value of m located at the left and the right hand-sides represent the bladed disk assembly itself and have exactly the same system properties as in the case of tuned bladed disks. Both of them are grounded with a spring whose stiffness value is k and have cross coupling between each other's x and y directions with a stiffness value of k_{12}. These springs physically represent the stiffness of large disks attached to rotor shaft and provide the coupling between vibrating bodies. It should also be noted that the motion of each mass in x and y directions are also coupled with a stiffness value of k_{xy}. These springs are also attached here to simulate and to capture the blade dynamics in this simple system. Each body has one contact point located on an inclined

surface with the damper that is pressed against to the vibrating bodies with a static pre-load, F^0. This load corresponds to the centrifugal force that presses the damper to the blades in turbo-machinery applications. The damper itself is modeled as a free body without applying any boundary condition, allowing for rigid body motions. Its x and y displacements are also coupled to each other by means of a spring with a value of k_D, which is not explicitly sketched in Fig. 10 for a clear view. Its image can be visualized exactly the same as the spring with stiffness k_{xy}, but on the damper. k_D physically corresponds to internal stiffness of the free wedge damper that involves into the bladed disk system as a secondary structure. A more compact expression of the generalized coordinates, linear system and damper matrices (with subscription D) and dynamic excitations are as follows;

$$\mathbf{q}=\begin{Bmatrix} x_1 \\ y_1 \\ x_2 \\ y_2 \end{Bmatrix},\quad \mathbf{M}=\begin{bmatrix} m & 0 & 0 & 0 \\ 0 & m & 0 & 0 \\ 0 & 0 & m & 0 \\ 0 & 0 & 0 & m \end{bmatrix},\quad \mathbf{C}=\begin{bmatrix} c & 0 & 0 & 0 \\ 0 & c & 0 & 0 \\ 0 & 0 & c & 0 \\ 0 & 0 & 0 & c \end{bmatrix},$$

$$\mathbf{K}=\begin{bmatrix} k+k_{xy}+k_{12} & -k_{xy} & -k_{12} & 0 \\ -k_{xy} & k+k_{xy}+k_{12} & 0 & -k_{12} \\ -k_{12} & 0 & k+k_{xy}+k_{12} & -k_{xy} \\ 0 & -k_{12} & -k_{xy} & k+k_{xy}+k_{12} \end{bmatrix},\quad \mathbf{F}_{exc}=\begin{Bmatrix} F_{x,1} \\ F_{y,1} \\ F_{x,2} \\ F_{y,2} \end{Bmatrix}.$$

$$\mathbf{q}_D=\begin{Bmatrix} x_D \\ y_D \end{Bmatrix},\quad \mathbf{M}_D=\begin{bmatrix} m_D & 0 \\ 0 & m_D \end{bmatrix},\quad \mathbf{C}_D=\begin{bmatrix} 0 & 0 \\ 0 & 0 \end{bmatrix},\quad \mathbf{K}_D=\begin{bmatrix} k_D & -k_D \\ -k_D & k_D \end{bmatrix},\quad \mathbf{F}_{exc,D}=\begin{Bmatrix} 0 \\ 0 \end{Bmatrix}.$$

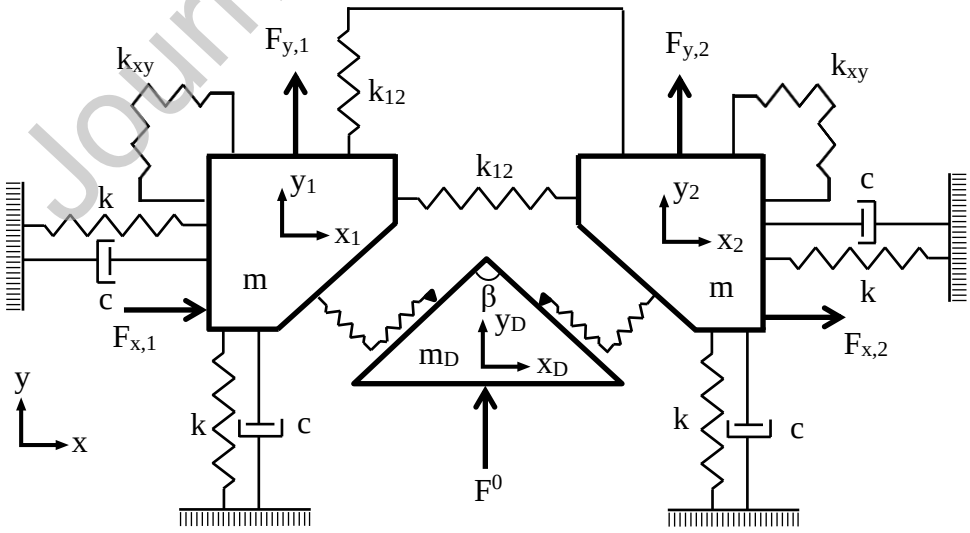

Fig. 10 Full View of the Lumped Parameters System

The model is harmonically forced in y and x directions from the first and the second masses, respectively. This type of forcing is intentionally applied in order to excite several modes of the system. Therefore, it enables to investigate the damper kinematics and the variability of the nonlinear responses under different contact conditions. All of the system parameters are given in Table 1. It should be noted that despite the model simplicity, it can be considered as a general framework for the construction of highly specialized and detailed FE models of mechanical structures having joint interfaces and showing frictional behaviors.

Table 1 Lumped System and Excitation Parameters

Parameter	Value	Parameter	Value	Parameter	Value
m	1 kg	k	$3*10^5$ Nm^{-1}	$F_{x,1}$	0
m_D	0.1 kg	k_{xy}	$3*10^5$ Nm^{-1}	$F_{y,1}$	$20\sin(\omega t+\pi)$ N
c	20 $N(m/s)^{-1}$	k_{12}	$7*10^5$ Nm^{-1}	$F_{x,2}$	$5\sin(\omega t)$ N
		k_D	$3*10^5$ Nm^{-1}	$F_{y,2}$	0

The geometry of the damper model is intentionally selected as isosceles triangle with an apical angle β and base angles α as shown in Fig. 11. This configuration gives an opportunity to examine the more general cases in which the static pre-load applied to the damper is not normal to the contact points. Furthermore, all the generalized coordinates will be coupled through this geometry in both x and y directions, which represents more realistic case scenario of real life applications with wedge dampers. It should also be noted that, in this way, a parametric study of the effect of different design alternatives by varying the angles β and α is also studied in this paper. The contact elements utilized in both sides share the same tangential (k_t) and normal (k_n) contact stiffness with a value $3*10^5$ Nm^{-1}. Coefficient of friction (μ) is taken 0.5. Fundamental harmonic is utilized in the dynamic balance equations.

Dynamic contact forces generated on the contact points are shown in Fig. 11. It should be noted that a coordinate transformation is needed from global to local in order to be able to calculate correct relative displacements and contact forces. The local coordinate systems (with superscription r) used in the calculations are also shown in Fig. 11. The transformations for both sides are applied as

$$\begin{Bmatrix} x_1^r \\ y_1^r \end{Bmatrix} = \begin{bmatrix} \cos(\alpha) & \sin(\alpha) \\ -\sin(\alpha) & \cos(\alpha) \end{bmatrix} \begin{Bmatrix} x \\ y \end{Bmatrix} \quad \text{and} \quad \begin{Bmatrix} x_2^r \\ y_2^r \end{Bmatrix} = \begin{bmatrix} \cos(\alpha) & -\sin(\alpha) \\ \sin(\alpha) & \cos(\alpha) \end{bmatrix} \begin{Bmatrix} x \\ y \end{Bmatrix}. \tag{16}$$

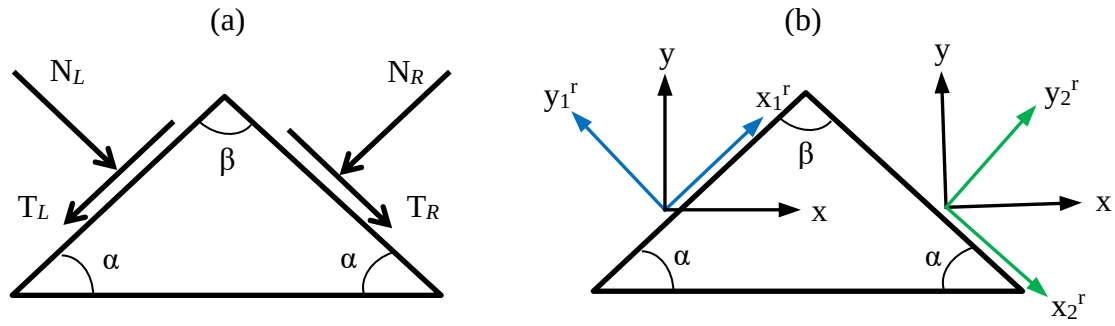

Fig. 11 (a) Contact Forces on Damper, (b) Coordinate Systems

4.2 Multiple Responses and Limits

As mentioned in Section 3.2 that there should be a cross coupling between the tangential and the normal forces in the contacts in order to obtain multiple response phenomena. For this purpose, the generalized coordinates in the system are coupled to each other with the stiffness k_{xy}. In addition, the apical angle, β, and base angles, α, in the following analyses are set equal to 120° and 30°, respectively; which provides a damper induced cross coupling into to the system as generally explained in Eq. (11). In this way, the coupling strength that directly affects the multiple response range is increased. Intensity of the coupling effect due to different geometries on response variability will be investigated in Section 4.3, as well. The following results are presented for the generalized coordinate of the right mass vertical displacement, y_2.

Fig. 12 depicts the displacement amplitudes of the free linear (without damper) and fully stuck linear (with damper) cases for the entire frequency range. All the mode shape sketches of the free linear case are also shown in Fig. 12. Additionally, eigenvector values for each mode are also presented in Table 2 for a better visualization of the system dynamics. The first mode is the one where in-phase motion takes place in the all coordinates. Thus, the insertion of the damper for this mode is not effective at all since there is no relative displacement between the DOFs. Natural frequency for the first mode also slightly decreases due to the extra damper mass. However, for the second mode, although the system makes an in-phase motion with respect to x_1–x_2 and y_1–y_2 directions, out-of-phase motions that take place in x_1–y_1 and x_2–y_2 coordinates provides a relative displacement due to cross-coupling provided by stiffness k_{xy}. Hence, the damper affects the linear system and introduces stiffness as in the cases of the third and the fourth modes, where the out-of-phase motions between the generalized coordinates are much clearer.

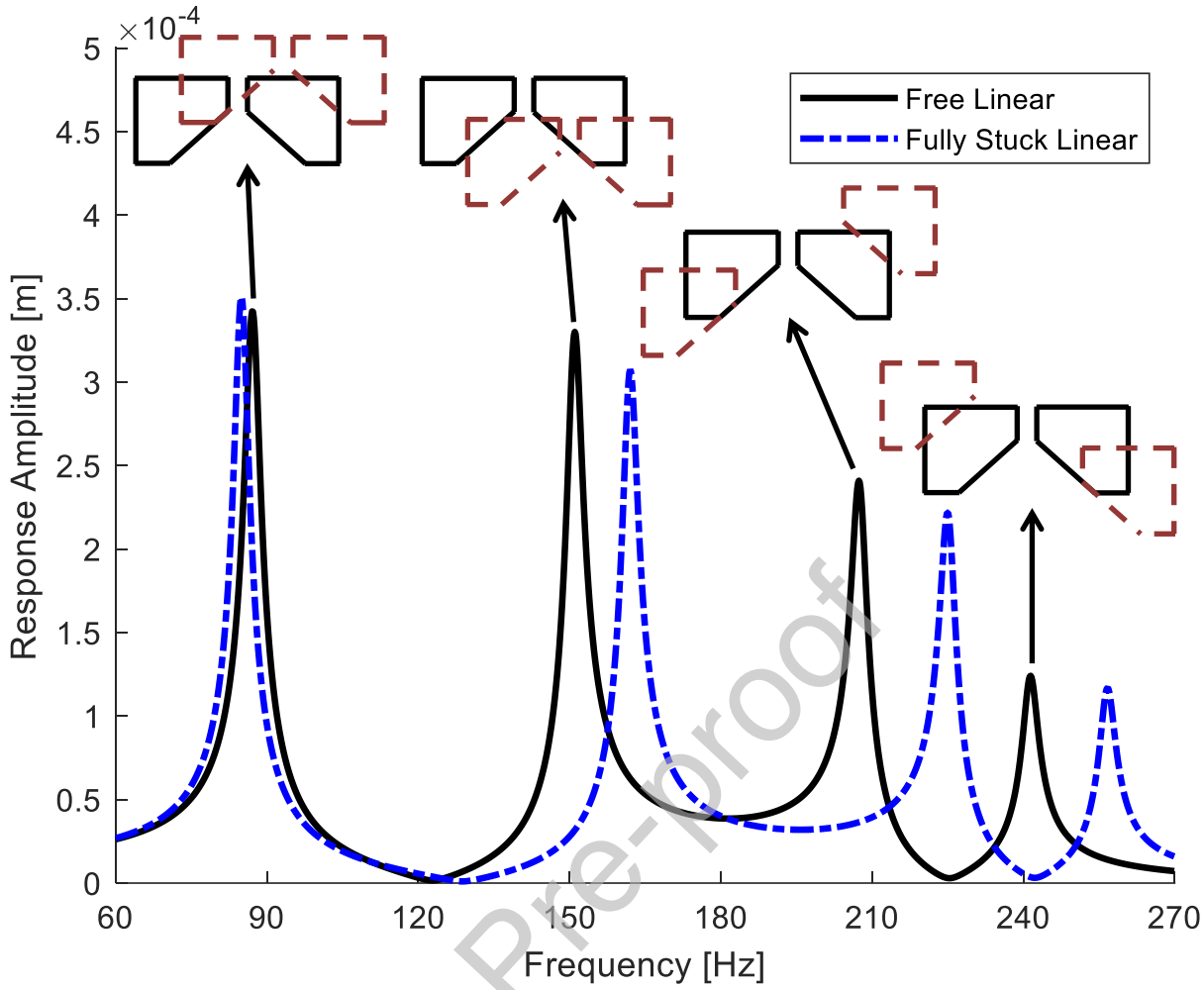

Fig. 12 Two Linear Cases Without and With the Damper

Table 2 Eigenvector Values for each Mode

Generalized Coordinates	1st Mode	2nd Mode	3rd Mode	4th Mode
x_1	1	1	-1	-1
y_1	1	-1	-1	1
x_2	1	1	1	1
y_2	1	-1	1	-1

Fig. 13 shows the displacement amplitudes of the free Linear Response (LR), fully stuck LR and Nonlinear Responses (NLR) around the second and the third resonance regions. Initial pre-load applied on the damper, F^0, is 120 N for each nonlinear case, which can be considered as a relatively high value and a moderate value for the second and the third resonances, respectively. This is expected since the dynamic external forces mostly excite the system's third mode. The damper efficiently dissipates the energy and damps the response in both resonance regions. However, it should be noted that the nonlinear responses shown in Fig. 13 are obtained for the totally same system without changing any input parameters. Although the

displacement amplitudes computed around the second resonance overlap with each other, they vary in the third resonance region, which shows multiple solutions exist. It is worth noting that the iterations during the nonlinear analysis for each curve within the range are fully converged, which makes all the solutions true as explained in Section 3.2. The only parameter that is changed for each analysis is the initial guess of the tangential force for AFT scheme before starting the computation of the contact forces. Five different initial values for $T(t)$ at $t = t_{ini}$ within the range of $\mu N(t)$ and $-\mu N(t)$ as shown in Fig. 5 end up with five particular converged responses, where the boundaries are indicated with red and brown curves, respectively. The upper and the lower response limits are calculated by using the numerical technique that is offered with this paper and based on the limit tangential force criteria as explained in Section 3.3. The limiting cases, which give the boundaries, correspond to nonlinear analyses performed with $T_{max}(t)$ and $T_{min}(t)$, that are ensured to obtain by assigning the initial guess values as the limits ($\mu N(t_{ini})$ and $-\mu N(t_{ini})$) for $T(t)$, respectively, as explained in Eqs. (14) and (15). The other three curves staying within the range are obtained by using three intermediate arbitrary initial values for $T(t)$, which results to three different contact forces at steady state with the values of $T_{int1}(t)$, $T_{int2}(t)$ and $T_{int3}(t)$.

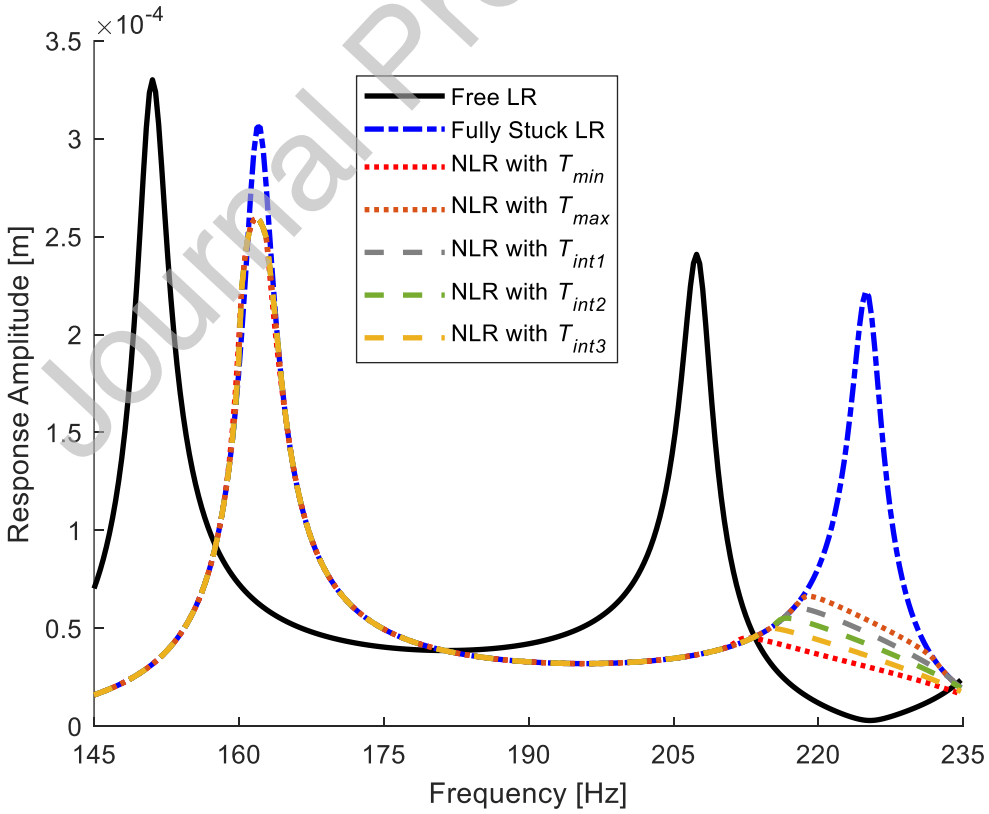

Fig. 13 Nonlinear Responses around the Second and the Third Resonance Regions

It is interesting to note that the multiple solutions exist only around the third resonance region, which shows the uncertainty phenomenon of the tangential forces is not observed for the second resonance region. This phenomenon occurs due to different contact conditions, which changes the effective stiffness and the equivalent damping terms of the contact elements for particular resonances. For a better illustration, consider Fig. 14 depicting the response graphs including the steady-state contact states of the both dry friction elements throughout the frequency range considered in the nonlinear analysis. It is worth noting that the initial guesses of the tangential force in these analyses are assigned as an arbitrary value which is representatively selected among an infinite number of possible alternatives within the range. Fig. 14a depicts one of the multiple displacement curves around the third resonance region, where the first contact is under fully stuck condition for the entire frequency interval while the other contact makes an alternating stick–slip motion for a specific range. In a more detailed explanation, red circles represent the frequency points where both contacts are fully stuck; while green stars stand for the frequencies in which one of the contact elements slips during its cycle. As explained in Section 3.2, the uncertainty of the first contact element's tangential force leads to obtain non-unique solutions for the frequency range shown by green stars. However, the second resonance region shown in Fig. 14b shows that the first and the second contact elements make an alternating stick–slip and an alternating stick–slip–lift-off motion, respectively, for the frequency points highlighted by blue squares. These contact states removes the uncertainty phenomenon as shown in Fig. 7 and Fig. 8 since the friction forces become unique. Hence, the effective stiffness and the equivalent damping of the contact elements obtained are the same for any initial guess value, which provides to compute a unique response at steady state.

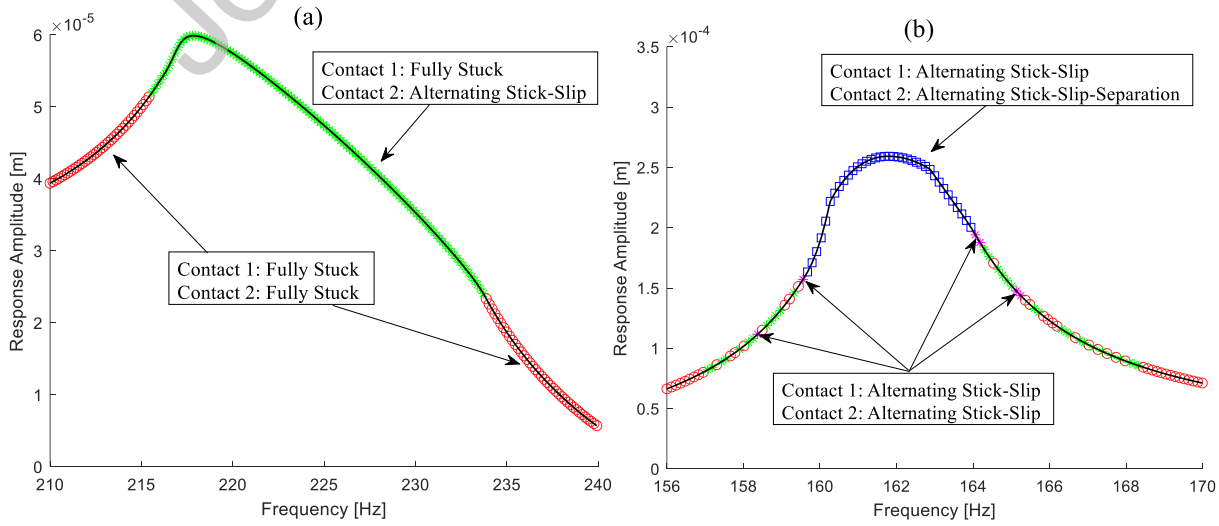

Fig. 14 (a) Contact States around the Third Resonance Region, (b) Contact States around the Second Resonance Region

In Fig. 15a, a general behavior of the nonlinear response curve corresponding to different static pre-loads applied on the damper is shown. The response is damped for the second and the third resonance regions as the pre-load decreases. The variability range is also highlighted around the third resonance region. It is seen that the range creates a closed region for relatively high pre-loads (400 N and 130 N). It shrinks with decreasing pre-loads and totally disappears after a certain value (60 N in this case). In order to explain this, it is worth mentioning that the effect of static pre-load on the maximum vibration amplitude is not regular. In particular, the maximum response amplitude starts decreasing with larger pre-loads from free linear case up to an optimum value, as shown in Fig. 3a. This observation is specific for low pre-loads. If the pre-load values keep rising beyond the optimum value, the response starts increasing again up to the fully-stuck case, where the system behaves as a linear one and no friction damping is provided by the damper. On the other side, the effect of static pre-load values on the resonance frequency is regular, where its value always increases as the pre-load becomes larger. As a result, for relatively high pre-loads (as 130 N and 400 N in Fig. 15a), the upper and the lower response boundaries clearly create a closed region (colored in purple and green) where intermediate response will end up to. On the other hand, for moderate pre-loads (60 N) at which the system would vibrate nearby the optimum configuration, the behavior is more complicated. The boundary response that corresponds to T_{max} is located on the right-hand side of the optimum, while the boundary response that corresponds to T_{min} stays on the left side, as shown in Fig. 15b. In this case, it is not possible to clearly identify a closed region where the intermediate responses will end up to. For instance, the resonance amplitudes of two intermediate curves computed by setting $T = T_{int1}$ and $T = T_{int2}$ lie outside the envelope of the two boundary responses. It should be stated that such a transition region is perfectly in line with the physics of frictionally damped dynamic systems.

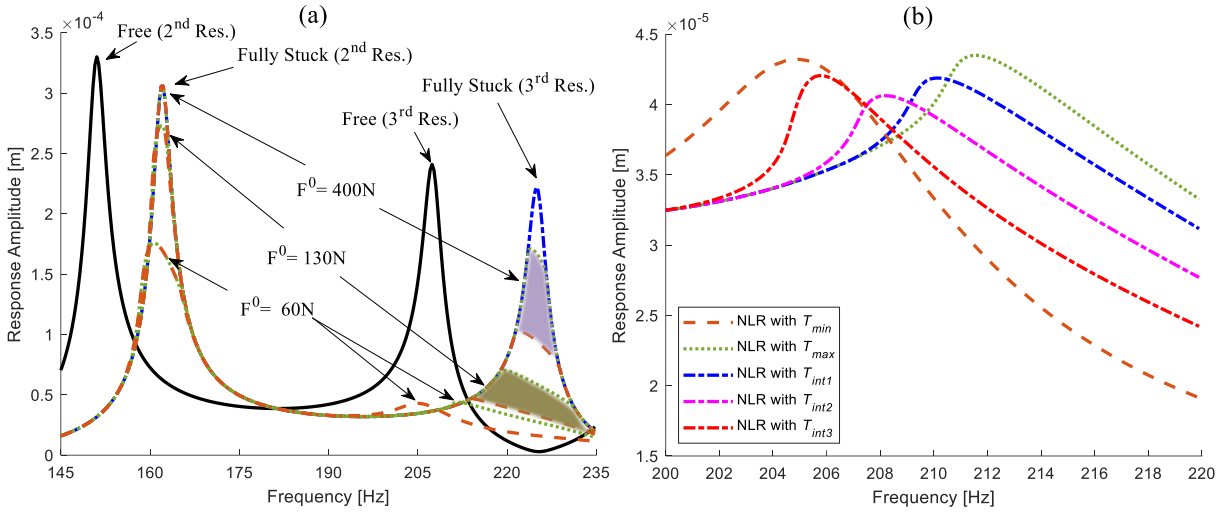

Fig. 15 (a) Nonlinear Responses for Different Static Pre-loads, (b) Nonlinear Responses for a Moderate Static Pre-Load, F^0 = 60N, nearby the optimum conditions

Fig. 16a shows the limits of the optimal curve around the third resonance region. It can be seen that the maximum amplitude starts from the free linear case with low pre-loads and saturates at the fully stuck linear case with high pre-loads. The response range varies considerably, showing the uncertainty may result in huge differences in the maximum response amplitudes. As previously explained, optimal curves have a local minimum, the so-called optimum point, around 45-80 N, which corresponds to the transition region shown in Fig. 15b. A closer view for this interval with three additional curves representing the ones obtained with intermediate values is given in Fig. 16b. Due to the non-regular relationship between the pre-load and the maximum response amplitude, the two response boundary do not represent the maximum and the minimum limits at each frequency. Nevertheless, the response boundaries allow determining the range of static pre-load values at which the optimum response is expected. Fig. 16c shows five different hysteresis curves obtained for the same static pre-load, F^0 = 80N at the corresponding resonance frequencies. It can be seen that the slipping contact element has completely different hysteresis curves corresponding to the limits and some other intermediate tangential force values of the sticking element. This indicates that different transition points with non-unique tangential forces change the damping characteristic of the overall system since k_{eq} and c_{eq} eventually become different for each case. The resonance frequency limits are also shown in Fig. 16d. The lower and the upper limits start from the same initial resonance value since both of the contacts tend to make an alternating stick–slip motion for relatively low pre-loads. This condition removes the uncertainty phenomenon and allows computing a unique response. Similarly, the limits overlap each other for high pre-loads at the fully stuck linear resonance frequency.

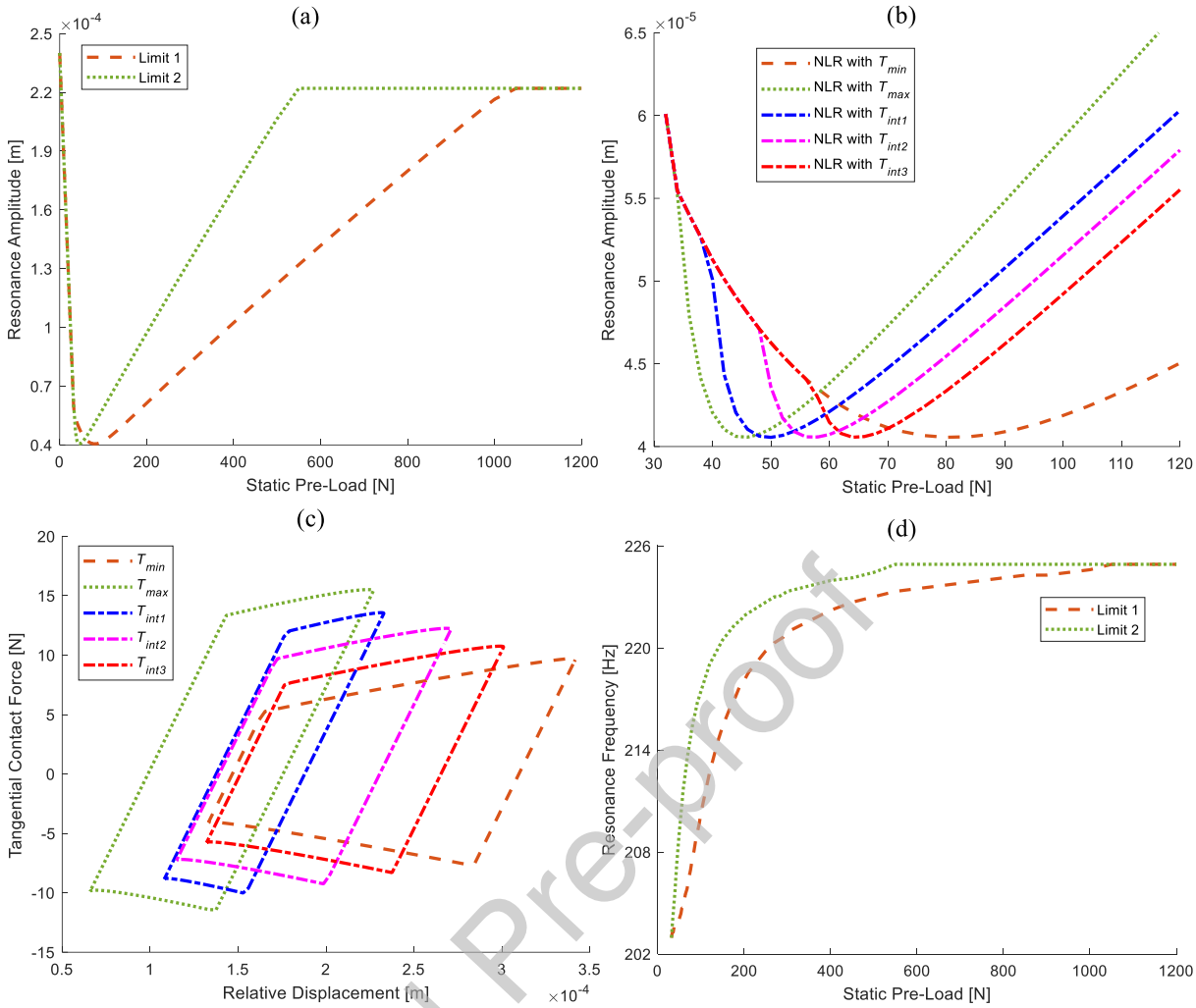

Fig. 16 (a) Optimal Curve Limits, (b) Optimal Curves for a Smaller Pre-Load Range, (c) Hysteresis Curves for a Static Pre-Load, F^0 = 80N, (d) Resonance Frequency Limits

4.3 The Effect of Damper Geometry on Multiple Responses

In this section, the effect of different damper geometries by changing the apical angle, β, and base angles, α, on multiple response behavior and limits is investigated.

Damper induced cross coupling is directly determined by β and α. As the damper geometry changes, the interaction between the tangential and the normal forces varies as shown in Eq. (11). For this purpose, β and α are firstly set equal to 180° and 0°, respectively, where the damper becomes perfectly flat in horizontal direction. Fig. 17a depicts the fully stuck linear and nonlinear displacement amplitudes around the third resonance region. Nonlinear response graphs represent the upper and lower limits of the variability range. The lower the static pre-load is, the more damped response obtained, as expected. However, comparing with the previous situation where β = 120°, the response variability in this case is extremely low. Almost unique response is obtained at steady-state whichever initial guess value is used in the

tangential force calculation. Because, the damper induced cross coupling is completely removed with flat damper and only interaction between x and y coordinates are provided by stiffness k_{xy}. Hence, the range for the multiple responses reduces substantially. Response variability is only obtained around limited regions where one of them is enlarged for a closer view in Fig. 17a. Fig. 17b shows the contact states during the nonlinear analysis performed with F^0 = 250N. It should be noted that the removal of damper induced cross coupling provides to obtain an alternating stick–slip motion in both contacts, which almost vanishes the uncertainty phenomenon and ends up to an unique response. The only frequency points in which the uncertainty is observed are the ones where one of the contacts is fully stuck while the other one makes an alternating stick–slip motion, which is highlighted with green stars. Multiple responses are possible for these small regions where one example is shown with a closer view in Fig. 17a.

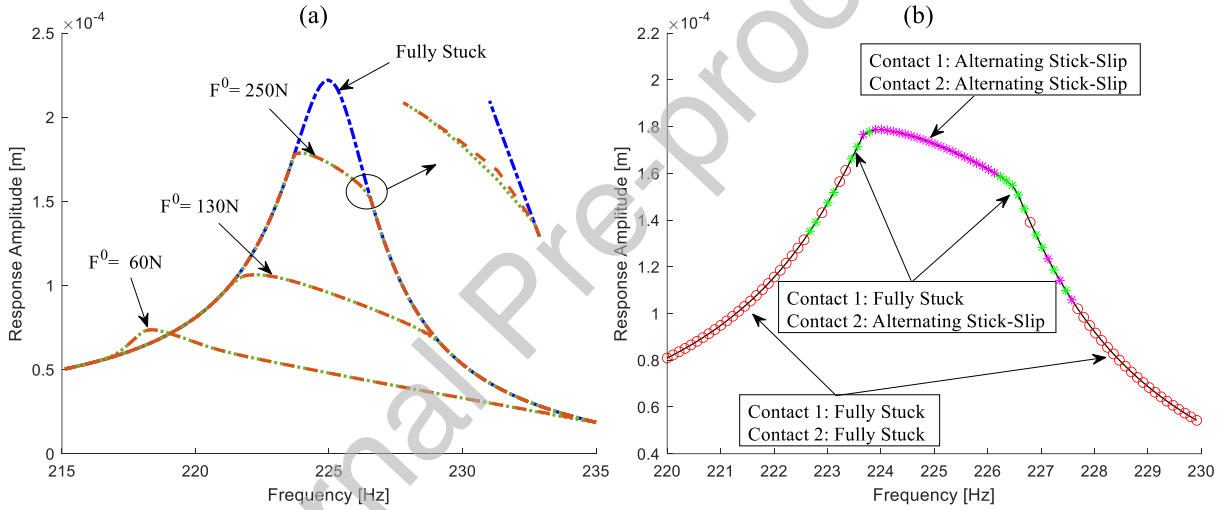

Fig. 17 (a) Nonlinear Responses for Flat Damper with Different Static Pre-loads, (b) Contact States around the Third Resonance Region with the Static Pre-Load, F^0 = 250N

Fig. 18a presents a more general view about the range of the variability in the frequency response with different apical angles, β, for the values higher than 90°. The upper and the lower curves with the same color for the same angles represent the limits. It is noted that as the apical angle increases from 90° to 180°, i.e. from isosceles right triangle shape to flat damper geometry, the response variability range decreases substantially. The largest range is obtained in case of 90° apical angle due to the fact that the damper induced cross coupling in contact forces is the most effective on the uncertainity phenomenon with this geometry. On the other hand, the response is almost obtained unique when β is 180°. Moreover, it should be noted that there is no monotonic decrease in the variability range as β increases from 90° to 180°. The range obtained when β = 160° is larger than the one obtained with β = 150° as can

be seen in the closer view shown in Fig. 18a. This indicates that the change of the damper geometry with different angles is not the only parameter affecting the pattern of the variability range. This observation leads that the static and the dynamic parts in the force balance equations cannot be separated in order to make a prior prediction for the behavior of the variability range. Full dynamic analysis is required to correctly observe the pattern change in the range with different geometries. It is also worth noting that all the nonlinear analyses for different angles in Fig. 18a are performed with particular pre-defined static pre-loads applied on the damper. The change of the variability range in optimal curves is also given in Fig. 18b, where the resonance displacement amplitudes are shown with increasing static pre-load. The upper and the lower limits for the flat geometry, i.e. β = 180°, lies on the same line. They start getting separated from each other as the angle decreases and the range reaches to the maximum width when β = 90°. However, the same non-monotonic behavior as in the case of frequency response graph is valid here, as well. The range for β = 150° is larger than the one obtained for β = 160°, which breaks the monotonic behavior in the variability pattern. It should also be noted the higher pre-loads provide to obtain the wider range while all the curves show similar behaviour for relatively low pre-loads that is squeezed in a narrow region. The reason for this fact is that both contacts tend to have an alternating stick–slip or an alternating stick–slip–lift-off motion under a low static pre-load, which removes the uncertainty and results with unique response.

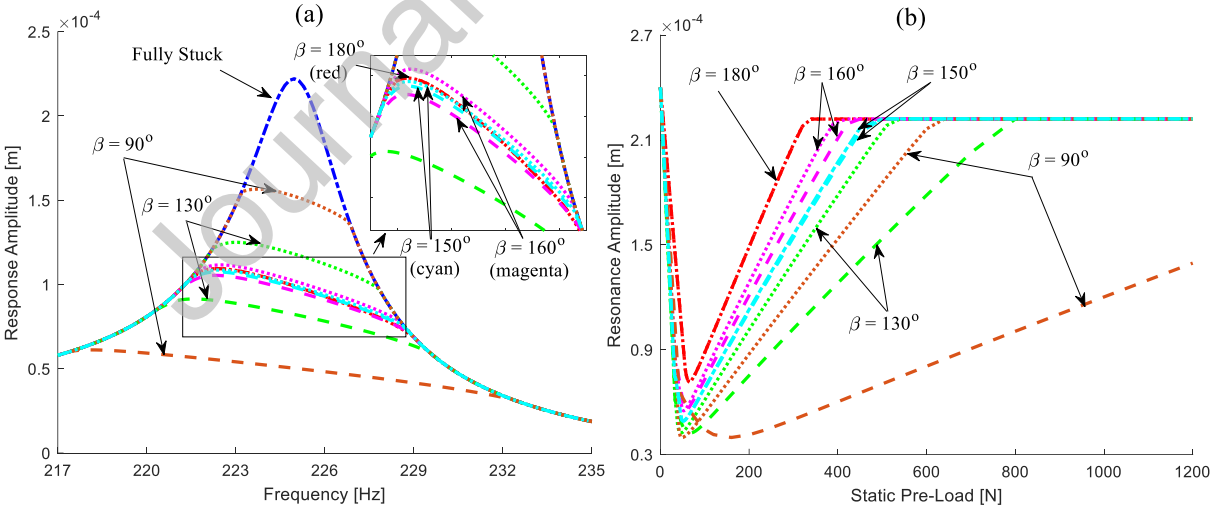

Fig. 18 (a) The Change of Variability Range in Frequency Response and (b) in Optimal Curves with Different High Apical Angles, β

Fig. 19a illustrates a straight diminishing behavior in the variability range as the apical angle, β, decreases from 90°. This shows that the effect of damper induced cross coupling on the uncertainty weakens with reducing β values. However, it is worth noting that when β is set

equal to a value lower than 90°, increasing static pre-load makes the damper tend to have more slip motion instead of stick, as opposed to the previous cases. Because, in this case, the pre-load applied on the damper contributes to the tangential component of the contact force more than the normal force direction due to the orientation of the simple system used. Hence, the contacts between the damper and the system are totally lost after a certain value. In order to overcome this problem, in addition to the static pre-load exerted on damper, another static pre-load is applied on the first and the second masses in x_1 and $-x_2$ directions, respectively. In this way, it is simulated that the masses are pressed through the damper and the damper is squeezed in between the masses, which enables to have stick state and keeps the damper in contact with the system during the periodic motion. It is also worth noting that this type of force enforcement is applied in many applications of vehicle dynamics for the structures with wedge dampers. Resonance amplitude limits with respect to varying static loads applied on the masses, not on the damper, are presented in Fig. 19b. These curves are defined in this study as pseudo-optimal curves, where the initial pre-load applied on the damper is kept constant at 500N. The variability range becomes smaller with decreasing apical angle as obtained in Fig. 19a. It should also be noted that the upper and the lower limits for each β value are parallel to each other since the pre-load on the damper is not a variable parameter anymore, which makes the response variability range constant with increasing pre-load until to reach fully stuck linear resonance response value.

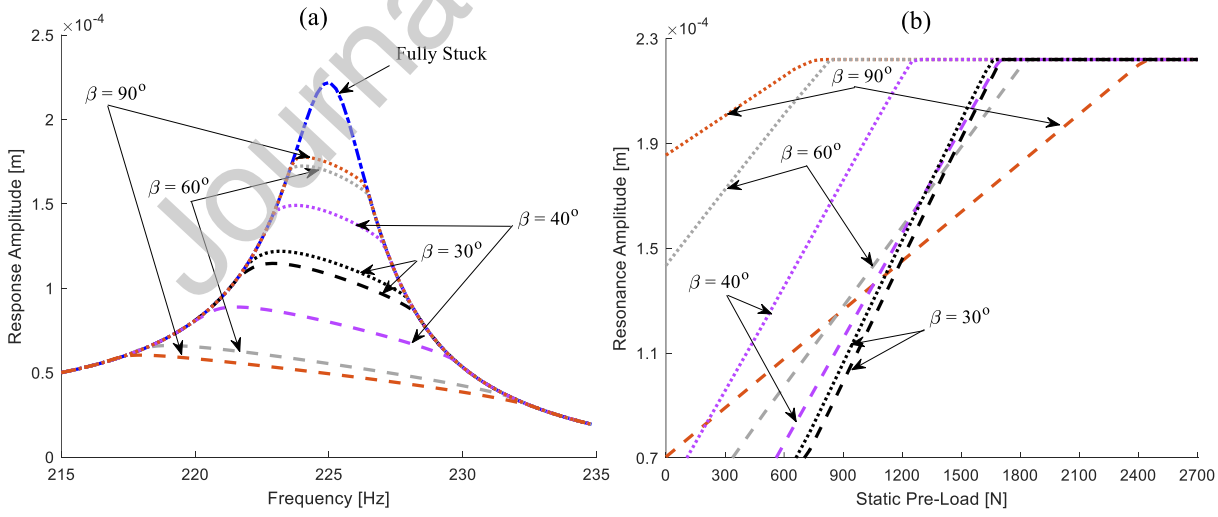

Fig. 19 (a) The Change of Variability Range in Frequency Response and (b) in Pseudo-Optimal Curves with Different Low Apical Angles, β

5. CONCLUSION

The uncertainty phenomenon in dry friction may result to obtain quite different dynamic response levels for the mechanical structures having contact interfaces, specifically for the wedge damper applications. Although the response variability has been firstly introduced more than two decades ago, further studies performed in the literature for this issue have become very limited. The existence of multiple solutions requires predicting the upper limit in terms of engineering point of view. Complying with this purpose, in this paper, a numerical approach for the determination of dynamic response limits among multiple solutions is offered. The method focuses on the mechanical systems with a wedge damper that is modeled by using a macro-slip friction element in each contact side.

The limiting cases of the variable response curves are determined with respect to the limit tangential forces. The uncertainty resulted by different possible tangential force values is confined to only one damper side whose contact element is fully stuck while the other side is making an alternating stick–slip or an alternating stick–slip–lift-off motion. In this case, use of two limit tangential forces in fully stuck element provides to obtain two extreme contact configurations on the other slipping side, which are the closest ones to free and stuck conditions. Hence, the upper and the lower limits for the dynamic response can be computed. The method is demonstrated on a lumped system representing a simplified version of vibrating blades with a wedge damper pressed in between them. Several case studies are presented by showing the response boundaries computed with the proposed approach. It is demonstrated that a large dynamic response variability, where the resonance amplitude of the upper boundary is 3 times of the lower one, exists for some particular cases. On the other hand, the change in resonance frequencies looks limited, when compared to amplitude variability. The highest variability in the resonance frequency change is observed up to 3% in this study. Parametric investigation of different configurations also shows that the variability range substantially changes with different damper geometries. The most variable results are obtained when apical angle, β, is set equal to 90° (isosceles right triangle geometry). The variability range decreases with flattening dampers. This observation clearly implicates that although the variability pattern is not perfectly monotonic, it is greatly affected by the damper induced cross-coupling due to the geometry of the damper. It can be said that the effect of the uncertainty can be minimized by using flat dampers, where the cross-coupling between the two damper sides is very low and the response variability decreases.

Despite the model simplicity, this paper presents the first numerical technique that can be utilized to determine the dynamic response limits among multiple solutions, according to the best of the authors' knowledge. However, the uncertainty phenomenon still requires much more attention with further studies. For example, inclusion of multiple contact points with more realistic structures and investigation of cases with modal interaction or internal resonances are still open research areas. Today's high order models may include thousands of contact points. The uncertainty in these structures becomes much more complex since the combination of different possible non-unique tangential forces brings theoretically an infinite number of different cases. The search for the response boundaries becomes a more challenging mathematical problem and the use of limit tangential force values, under those circumstances, may not be suitable to determine the boundaries of the response variability. Nonetheless, the authors think that the researchers and analysts would become much more aware about the uncertainty phenomenon and the response limits with this study.

APPENDIX

Analytical expression of equivalent stiffness and damping terms for a 1D Jenkins element which is under a single harmonic input motion ($q(t)=\hat{q}\cos(\omega t)$) with a constant normal load, N_0, can be written as

$$\mathrm{k}_{eq}=\begin{cases} k_t & \text{full stick} \\ \dfrac{k_t}{\pi}\left(\varphi-\dfrac{\sin(2\varphi)}{2}\right) & \text{stick-slip} \end{cases} \quad \text{and} \quad \mathrm{c}_{eq}=\begin{cases} 0 & \text{full stick} \\ \dfrac{4\mu N_0}{\pi\hat{q}}\left(1-\dfrac{\mu N_0}{k_t\hat{q}}\right) & \text{stick-slip} \end{cases}, \tag{17}$$

where

$$\varphi=\arccos\left(1-\frac{2\mu N_0}{k_t\hat{q}}\right). \tag{18}$$

Declaration of interests

☒ The authors declare that they have no known competing financial interests or personal relationships that could have appeared to influence the work reported in this paper

Author statement

Erhan Ferhatoglu: Conceptualization, Methodology, Software, Validation, Visualization, Writing - Original Draft

Stefano Zucca: Conceptualization, Methodology, Supervision, Writing - Review & Editing

REFERENCES

[1] B.A. Cowles, High cycle fatigue in aircraft gas turbines - an industry prospective, Int. J. Fracture 80(2-3) (1996) 147-163. https://doi.org/10.1007/BF00012667.

[2] K.Y. Sanliturk, D.J. Ewins, A.B. Stanbridge, Underplatform dampers for turbine blades: theoretical modeling, analysis and comparison with experimental data, ASME J. Eng. Gas Turbines Power 123(4) (2001) 919-929. https://doi.org/10.1115/1.1385830.

[3] E.P. Petrov, Explicit finite element models of friction dampers in forced response analysis of bladed disks, ASME J. Eng. Gas Turbines Power 130(2) (2008): 022502. https://doi.org/10.1115/1.2772633.

[4] E. Cigeroglu, N. An, C.H. Menq, Forced response prediction of constrained and unconstrained structures coupled through frictional contacts, ASME J. Eng. Gas Turbines Power 131(2) (2009): 022505. https://doi.org/10.1115/1.2940356.

[5] A.B. Kaiser, J.P. Cusumano, J.F. Gardner, Modeling and dynamics of friction wedge dampers in railroad freight trucks, Vehicle Syst. Dyn. 38(1) (2002) 55-82. https://doi.org/10.1076/vesd.38.1.55.3519.

[6] J. Steets, B.J. Chan, C. Sandu, Multibody Dynamics Approach to the Modeling of Friction Wedge Elements for Freight Train Suspensions. I: Theory, J Transp. Eng. 136(8) (2010) 709-716. https://doi.org/10.1061/(ASCE)0733-947X(2010)136:8(709).

[7] C. Cole, M. McClanachan, M. Spiryagin, Y.Q. Sun, Wagon instability in long trains, Vehicle Syst. Dyn. 50(s1) (2012) 303-317. https://doi.org/10.1080/00423114.2012.659742.

[8] C. Cole, M. Spiryagin, Y.Q. Sun, Assessing wagon stability in complex train systems, Int. J. Rail Transp. 1(4) (2013) 193-217. https://doi.org/10.1080/23248378.2013.836396.

[9] Q. Wu, C. Cole, S. Luo, M. Spiryagin, A review of dynamics modelling of friction draft gear, Vehicle Syst. Dyn. 52(6) (2014) 733-758. https://doi.org/10.1080/00423114.2014.894199.

[10] W.D. Iwan, The dynamic response of bilinear hysteretic systems, PhD Thesis, California Institute of Technology, USA, 1961.

[11] J.H. Griffin, Friction damping of resonant stresses in gas turbine engine airfoils, J. Eng. Power 102(2) (1980) 329-333. https://doi.org/10.1115/1.3230256.

[12] T.M. Cameron, J.H. Griffin, R. E. Kielb , T. M. Hoosac, An integrated approach for friction damper design, J. Vib. Acoust. 112(2) (1990) 175-182. https://doi.org/10.1115/1.2930110.

[13] K.Y. Sanliturk, D.J. Ewins, Modelling two-dimensional friction contact and its application using harmonic balance method, J Sound Vib. 193(2) (1996) 511-523. https://doi.org/10.1006/jsvi.1996.0299.

[14] C.H. Menq, B.D. Yang, Non-linear spring resistance and friction damping of frictional constraint having two-dimensional motion, J Sound Vib. 217(1) (1998) 127-143. https://doi.org/10.1006/jsvi.1998.1739.

[15] B.D. Yang, C.H. Menq, Characterization of 3D contact kinematics and prediction of resonant response of structures having 3D frictional constraint, J Sound Vib. 217(5) (1998) 909-925. https://doi.org/10.1006/jsvi.1998.1802.

[16] Q. Wu, C. Cole, M. Spiryagin, Y.Q. Sun, A review of dynamics modelling of friction wedge suspensions, Vehicle Syst. Dyn. 52(11) (2014) 1389-1415. https://doi.org/10.1080/00423114.2014.943249.

[17] M. Krack, L. Salles, F. Thouverez, Vibration prediction of bladed disks coupled by friction joints, Arch. Comput. Methods Eng. 24 (2017) 589–636. https://doi.org/10.1007/s11831-016-9183-2.

[18] C.M. Firrone, S. Zucca, M.M. Gola, The effect of underplatform dampers on the forced response of bladed disks by a coupled static/dynamic harmonic balance method, Int. J. Nonl. Mech. 46(2) (2011) 363-375. https://doi.org/10.1016/j.ijnonlinmec.2010.10.001.

[19] S. Zucca, C.M. Firrone, M.M. Gola, Numerical assessment of friction damping at turbine blade root joints by simultaneous calculation of the static and dynamic contact loads, Nonlinear Dyn. 67 (2012) 1943-1955. https://doi.org/10.1007/s11071-011-0119-y.

[20] L. Pesaresi, L. Salles, A. Jones, J.S. Green, C.W. Schwingshackl, Modelling the nonlinear behaviour of an underplatform damper test rig for turbine applications, Mech. Syst. Signal Process. 85 (2017) 662-679. https://doi.org/10.1016/j.ymssp.2016.09.007.

[21] B.D. Yang, C.H. Menq, Characterization of contact kinematics and application to the design of wedge dampers in turbomachinery blading: part 1—stick-slip contact kinematics, J. Eng. Gas Turbines Power 120(2) (1998) 410-417. https://doi.org/10.1115/1.2818138.

[22] B.D. Yang, C.H. Menq, Characterization of contact kinematics and application to the design of wedge dampers in turbomachinery blading: part 2—prediction of forced response and experimental verification, J. Eng. Gas Turbines Power 120(2) (1998) 418-423. https://doi.org/10.1115/1.2818139.

[23] S. Zucca, D. Botto, M.M. Gola, Range of variability in the dynamics of semi-cylindrical friction dampers for turbine blades, Proceedings of the ASME Turbo Expo 2008: Power for Land, Sea, and Air. Volume 5: Structures and Dynamics, Parts A and B. Berlin, Germany. June 9–13, 2008. pp. 519-529. https://doi.org/10.1115/GT2008-51058.

[24] S. Zucca, C.M. Firrone, M.M. Gola, Modeling underplatform dampers for turbine blades a refined approach in the frequency domain, J. Vib Control 19(7) (2013) 1087-1102. https://doi.org/10.1177/1077546312440809.

[25] E. Ferhatoglu, S. Zucca, D. Botto, J. Auciello, L. Arcangeli, Nonlinear vibration analysis of turbine bladed disks with mid-span dampers, Proceedings of ASME Turbo Expo 2020: Turbomachinery Technical Conference and Exposition. Virtual, Online, September 21-25, 2020.

[26] M. Stender, M. Jahn, N. Hoffmann, J. Wallaschek, Hyperchaos co-existing with periodic orbits in a frictional oscillator, J Sound Vib. 472 (2020): 115203. https://doi.org/10.1016/j.jsv.2020.115203.

[27] D. Botto, M. Umer, A novel test rig to investigate under-platform damper dynamics, Mech. Syst. Signal Process. 100 (2018) 344-359. https://doi.org/10.1016/j.ymssp.2017.07.046.

[28] C. Gastaldi, J. Gross, M. Scheel, T.M. Berruti, M. Krack, Modeling complex contact conditions and their effect on blade dynamics, Proceedings of ASME Turbo Expo 2020: Turbomachinery Technical Conference and Exposition. Virtual, Online, September 21-25, 2020.

[29] B.D. Yang, Contact kinematics of friction interfaces and applications to the prediction of resonant response of frictionally constrained turbine blades. PhD Thesis, The Ohio State University, USA, 1996.

[30] L. Panning, W. Sextro, K. Popp, Spatial dynamics of tuned and mistuned bladed disks with cylindrical and wedge-shaped friction dampers, Int. J. Rotating Mach. 9(3) (2003) 219-228. https://doi.org/10.1155/S1023621X03000198.

[31] E.P. Petrov, D.J. Ewins, Advanced modeling of underplatform friction dampers for analysis of bladed disk vibration, J. Turbomach. 129(1) (2007) 143-150. https://doi.org/10.1115/1.2372775.

[32] C. Siewert, L. Panning, J. Wallaschek, C. Richter, Multiharmonic forced response analysis of a turbine blading coupled by nonlinear contact forces, J. Eng. Gas Turbines Power 132(8) (2010): 082501. https://doi.org/10.1115/1.4000266.

[33] E.P. Petrov, D.J. Ewins, Analytical formulation of friction interface elements for analysis of nonlinear multi-harmonic vibrations of bladed disks, J. Turbomach. 125(2) (2003) 364-371. https://doi.org/10.1115/1.1539868.

[34] M. Krack, J. Gross, Harmonic balance for nonlinear vibration problems, New York: Springer, 2019.

[35] T.M. Cameron, J.H. Griffin, An alternating frequency/time domain method for calculating the steady-state response of nonlinear dynamic systems, J. Appl. Mech. 56(1) (1989) 149-154. https://doi.org/10.1115/1.3176036.

[36] T.F.C. Chan, H.B. Keller, Arc-length continuation and multigrid techniques for nonlinear elliptic eigenvalue problems, SIAM J. Sci. and Stat. Comput. 3(2) (1982) 173-194. https://doi.org/10.1137/0903012.

[37] L. Peletan, S. Baguet, M Torkhani, G.J. Richardet, Quasi-periodic harmonic balance method for rubbing self-induced vibrations in rotor–stator dynamics, Nonlinear Dyn. 78 (2014) 2501-2515. https://doi.org/10.1007/s11071-014-1606-8.

[38] C.H. Menq, J.H. Griffin, A comparison of transient and steady state finite element analyses of the forced response of a frictionally damped beam, J. Vib., Acoust., Stress, and Reliab. 107(1) (1985) 19-25. https://doi.org/10.1115/1.3274709.

[39] O. Tanrikulu, B. Kuran, H.N. Özgüven, M. Imregun, Forced harmonic response analysis of nonlinear structures using describing functions, AIAA J. 31(7) (1993) 1313-1320. https://doi.org/10.2514/3.11769.

[40] D. Botto, C. Gastaldi, M. M. Gola, M. Umer, An experimental ınvestigation of the dynamics of a blade with two under-platform dampers, J. Eng. Gas Turbines Power. 140(3) (2018): 032504. https://doi.org/10.1115/1.4037865.